Journal of Materials Chemistry A

ROYAL SOCIETY OF CHEMISTRY

REVIEW

View Article Online
View Journal | View Issue

Cite this: J. Mater. Chem. A, 2025, 13, 18115

Triplet–triplet annihilation upconversion sensitized with nanocrystals for a new generation of photocatalytic systems

Michele Bucchieri,[ab] Francesca S. Freyria *[a] and Barbara Bonelli [a]

Photon upconversion (UC) is a quantum mechanical process that converts two (or more) lower-energy photons (typically in the NIR or visible range) into a higher-energy photon (in the visible or UV range, respectively). Triplet–Triplet Annihilation (TTA) is one of the most promising UC processes as it can occur directly under non-coherent sources, such as sunlight. The TTA mechanism requires a sensitizer and an annihilator, both of which are generally organic or organo-metallic dyes. Recently, novel TTA-UC systems sensitized with nanocrystals have been developed, offering significant advantages compared to molecular systems, such as the possibility of easily tuning their absorption and emission wavelengths across the solar spectrum and enhanced photostability. These TTA-UC systems are excellent candidates for a wide range of applications, including 3D printing, bioimaging and, especially, photovoltaics and photocatalysis. This review provides a comprehensive and up-to-date overview of the recent advances in the field, addressing the key challenges and current goals, such as maximizing the UC quantum yield. After outlining the principles and mechanisms of TTA, we focus on the main TTA components. Special emphasis is placed on TTA-UC systems sensitized with nanocrystals and their emerging applications, with particular attention to photo-driven reactions. Our aim is to inspire interest in future studies in this exciting yet still emerging subject.

Received 24th February 2025
Accepted 9th April 2025

DOI: 10.1039/d5ta01541c

rsc.li/materials-a

1. Introduction

Photon upconversion (UC) is an energy-shifting process through which two or more lower-energy photons (*e.g.* in the near infrared (NIR) or visible range) can be converted into one higher-energy photon (*e.g.* in the visible or UV range). Discovered for the first time by Parker and Hatchard in the early 1960s,[1] this phenomenon has recently gained attention in many fields, ranging from photovoltaics to photocatalysis, biological imaging, 3D printing, *etc.*[2] So far, the most known conversion of energy within materials is the counterpart mechanism where a higher energy photon is transformed into a lower energy one through a final radiative emission. This downshifting process is generally called photoluminescence (Scheme 1a). Another similar mechanism is downconversion (also called exciton fission process), in which a higher energy photon is converted into two or more lower energy photons. In rare-earth compounds this process is generally referred to as quantum cutting *via* energy transfer,[3] whereas singlet fission (SF) and multiple exciton generation (MEG) concepts are related to systems involving organic molecules and semiconductor nanocrystals (NCs), respectively (Scheme 1b and c).

In a typical downshifting process (Scheme 1a), an electron, generally in a singlet ground state, absorbs a photon, promoting a transition to a higher excited state. It then decays to lower excited states through non-radiative transitions, *e.g.* vibrational relaxation and intersystem crossing (ISC) with the conversion of a singlet to a triplet or the opposite. Finally, the electron returns to the ground state, emitting a photon with a lower energy compared to the original incident one *via* fluorescence or, in the presence of ISC transitions, *via* phosphorescence. Singlet fission is a downconversion process where one excited singlet state splits into two lower-energy triplet states and charge carrier states.

Conversely, the UC mechanism converts low-frequency (long wavelength) photons into high-frequency (short wavelength) photons (Scheme 1d). It can occur through different mechanisms, like higher-order harmonic generation, multiphoton absorption, phonon-assisted anti-Stokes emission, Auger recombination and, in the case of multicomponent systems like rare earth doped nanoparticles, through excited state absorption, energy transfer UC, collaborative sensitization upconversion and photon avalanche processes.[4] Among these mechanisms, upconversion achieved through the triplet–triplet annihilation (TTA, also called triplet fusion, TF)[5] process has recently drawn significant attention due to its ability to proceed under weak,

[a]Department of Applied Science and Technology and INSTM Unit of Torino Politecnico, Corso Duca degli Abruzzi 24, Torino 10129, Italy. E-mail: francesca.freyria@polito.it
[b]Department of Chemistry, Biology and Biotechnology, Università degli Studi di Perugia, Via Elce di Sotto 8, Perugia 06123, Italy

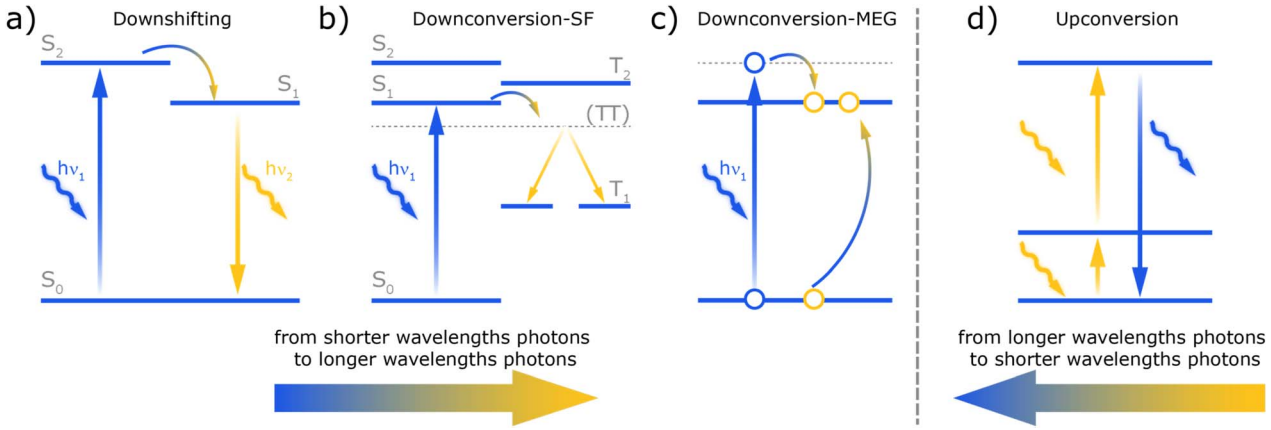

Scheme 1 Schematic diagrams of (a) a downshift process (*e.g.* photoluminescence), (b) a downconversion process (from which two triplet states/excitons are generated for one absorbed photon) such as singlet fission, and (c) multiple exciton generation; (d) generic UC processes; based on ref. 8–10.

non-coherent light sources, such as sunlight. Achieving this with other UC mechanisms is much more challenging.[6] An upconversion system (UCS) typically consists of a photosensitizer and an emitter. The photosensitizer's role is to absorb lower-energy light, transferring the excitation energy to the emitter, which then radiatively emits higher-energy radiation.[7]

Briefly, during the UC process (Scheme 1d), an electron, excited to state 1 by an incoming photon, is promoted to the high-energy excited state by interacting with another incoming photon or by an energy transfer process; finally, the excited electron will radiatively decay to the ground state emitting a photon with higher energy with respect to the two incoming ones, (*e.g.* from the NIR to the visible range or from the visible to the UV range).

The integration of the UC mechanism into devices can be truly groundbreaking. For instance, it could allow the human eye to "see" beyond the natural limits of 700 nm, by converting NIR light, a wavelength range typically invisible to our eye, into visible light through UC nanoparticles embedded into or directly bound to retinal photoreceptors or an optical lens.[11,12]

Currently, most UC systems rely on lanthanide-ion based nanoparticles, which show a good photostability and are able to

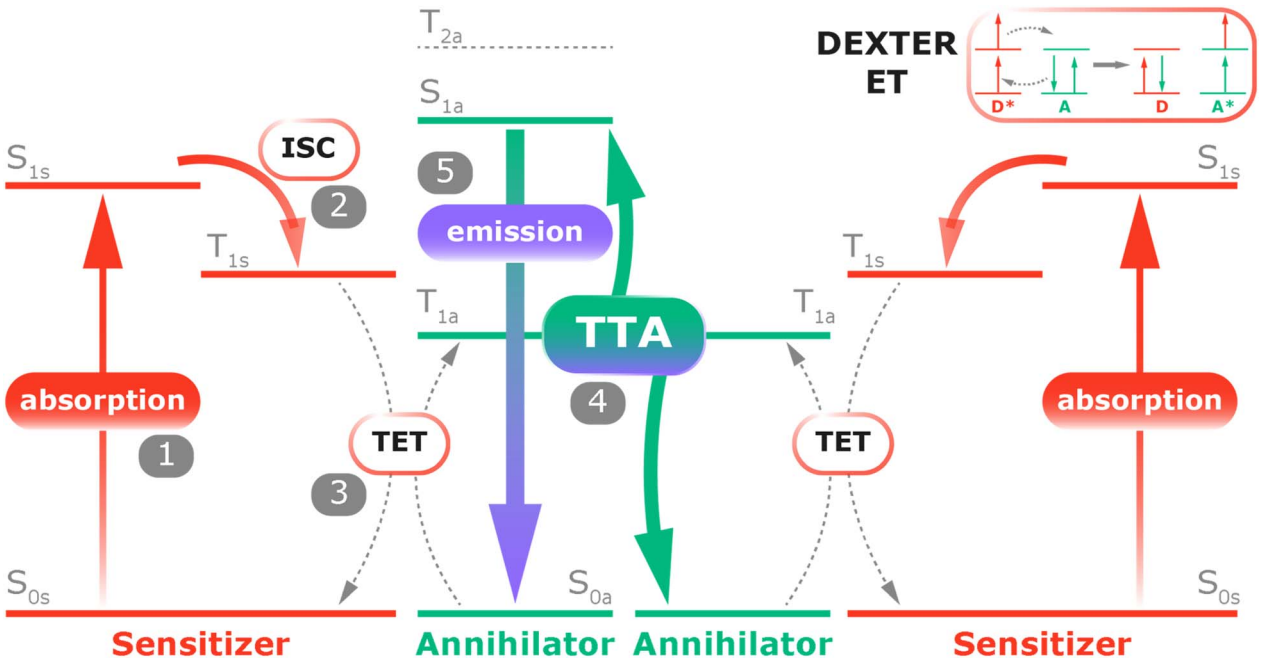

Scheme 2 Jablonski diagram demonstrating the TTA-UC *via* conventional triplet sensitization,[5,25,26] (1) photoexcitation of the sensitizer; (2) sensitizer ISC from the singlet state to the triplet state of the sensitizer; (3) triplet energy transfer between the sensitizer and the annihilator; (4) TTA process. (5) Emission of the upconverted photon. Inset: triplet–triplet Dexter energy transfer (ET), where D is the donor and A is the acceptor. The asterisk indicates the excited state.

provide a very sharp emission spectrum with large anti-Stokes shifts thanks to their long-lifetime f-electronic states in the ms regime.[2,13] These systems, however, suffer from low sustainability, a weak and narrow absorption and require high excitation intensity thresholds (W cm^{-2} to kW cm^{-2}) for efficient UC. These drawbacks have created the driving force to engineer new kinds of UC systems.[14]

The triplet–triplet annihilation process offers a promising alternative for achieving UC emission, due to its much lower excitation intensity requirements (~100 mW cm^{-2}) using incoherent light, making it very attractive for applications such as photocatalysis, solar cells and bioimaging.[15]

A typical triplet–triplet annihilation upconversion (TTA-UC) system is a nanocomposite material formed by using a photosensitizer and an annihilator/emitter (Scheme 2).[16,17] The seminal work in this field was conducted by Parker and Hatchard in 1962,[1] using organic chromophore pairs, with both absorption and emission in the UV/blue visible region. However, due to the low UC efficiency, further quenched by O_2, and the limited photostability of the organic moieties, the TTA-UC mechanism did not receive much attention from the scientific community for several decades.[13] In 2005, Castellano and co-workers revived interest for this process: they applied a Ru(II) metal–organic complex as a photosensitizer, paired with 9,10-diphenylanthracene (DPA) as the annihilator, developing a TTA-UC system in a colloidal solution able to convert green light into blue light.[7] The presence of the transition metal complex appeared to facilitate ISC from the excited singlet state to the lower-in-energy excited triplet state, improving the efficiency. They demonstrated that TTA-UC induced luminescence emission could be seen by the naked eye upon excitation with a commercial green laser at low power (<5 mW at 532 nm) and even under the direct excitation of non-coherent light, different from the conventional lanthanide-based UC systems. Starting from this pioneering work, several studies followed, adopting a great variety of organic dyes and metal–organic complexes as both sensitizers and annihilators. These advantages led to the development of TTA-UC systems able to emit luminescence across the entire solar spectrum, from the UV to the NIR, highlighting the great potential of these systems, especially for applications involving interaction with direct sunlight.[18–22] Building on this potential, understanding the fundamental working principles of TTA-UC systems is crucial for optimizing their performance for real-world applications.

2. Mechanisms of TTA-UC

In a classic TTA-UC system (Scheme 2), upon absorbing a low-energy photon, the sensitizer is excited from the ground state (S_{0s}) to its first singlet excited state (S_{1s}). This excited state undergoes intersystem crossing, leading to a transition to the energetically lower triplet excited state (T_{1s}). A process of triplet–triplet energy transfer (TET) then occurs, in which the sensitizer transfers its energy to the annihilator *via* Dexter-like energy transfer processes (inset of Scheme 2). Since this non-radiative electron exchange, which often occurs through intermolecular collisions, requires an orbital overlap between the sensitizer

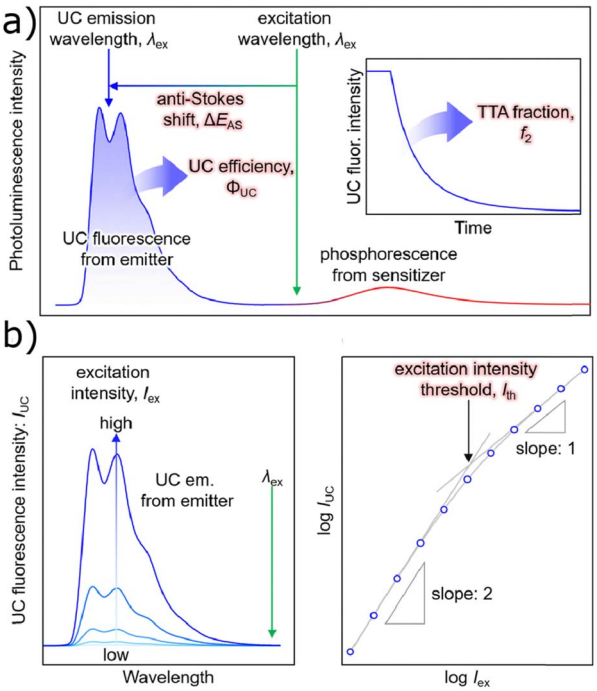

Fig. 1 (a) Simulated typical PL spectrum of a TTA-UC system. (b) Simulated graph of a typical UC spectrum as a function of the excitation intensity and simulated log-plot reporting the UC emission intensity as a function of the incident one; note the slope change in proximity to I_{th}. Reproduced from ref. 23 with permission from the Royal Society of Chemistry.

(the donor) and annihilator (the acceptor), the two of them must be within approximately 10 Å of each other, as the process efficiency decreases exponentially with distance. Subsequently, the collision of two annihilators, both in their triplet states (T_{1a}), leads to the formation of one emitter in the ground state and another one in an excited singlet state (S_{1a}). The latter excited emitter radiatively decays to its ground state, emitting a higher-energy photon (Fig. 1a).[24] This upconversion process requires that for effective singlet formation *via* TTA, the energy of the annihilator triplet excited state (T_{1a}) should exceed half the energy of the lowest emissive singlet state (S_{1a}) while ideally remaining below half the energy of the higher triplet states (*e.g.*, T_{2a}), as following $\frac{1}{2}S_{1a} \leq T_{1a} \leq \frac{1}{2}T_{2a}$.[25] This ensures that the energy from the two triplet states is sufficient to populate the singlet excited state, enabling the radiative decay with the emission of a higher-energy photon.[26]

2.1. Efficiency of the TTA-UC system

Since TTA is a two-photon process, its maximum quantum yield (QY) value can theoretically be expressed considering its two-photon nature (50%) or not (100%). Based on this distinction, the UC QY (Φ_{UC}) is capped at 50%, while the UC efficiency (Φ_{eff}) can extend to 100%. Unfortunately, many studies in the literature fail to clearly specify which metric is being reported. This lack of standardization complicates the comparison of TTA-UC systems used in different research experiments.[27,28] The Φ_{UC} can be defined as the ratio of the number ($n°$) of UC photons

emitted (or excited states generated)[23,27] to the number of photons absorbed by the sensitizer. Alternatively, it can be described as the product of the efficiencies of all the individual processes contributing to upconversion, as described by:

$$\Phi_{UC} = \frac{n^{\circ}\text{ UC emitted photons}}{n^{\circ}\text{ absorbed photons}} = \frac{1}{2}\Phi_{eff} = \Phi_{ISC}\Phi_{TET}\Phi_{TTA}\Phi_{F}f \quad (1)$$

In eqn (1) $\Phi_{ISC} = n^{\circ}T_s/n^{\circ}S_s$ is the intersystem crossing efficiency, defined as the ratio between the number of sensitizers in their triplet state (T_{1s}) and those in their higher-energy singlet state (S_{1s}), following interaction with incident light; $\Phi_{TET} = n^{\circ}T_s/n^{\circ}T_a$ is the efficiency of TET from the sensitizer (donor) to the annihilator (acceptor), depending on the relative energies of their triplet states; $\Phi_{TTA} = n^{\circ}S_a/n^{\circ}T_a$ represents the efficiency of forming emitters in the S_{1a} state from the collision of two annihilators in their triplet excited states T_{1a}; the f factor represents the statistical probability of forming an excited singlet state through the annihilation of two triplet states. Finally, Φ_F represents the efficiency of a radiative decay, after the formation of the emitter in the singlet state (S_{1a}), leading to UC emission.[23,29,30]

For an efficient ISC process, a sensitizer must display a sufficient energy gap (generally a few tenths of eV)[28,31] between its singlet excited state (S_{1s}) and its triplet state (T_{1s}). Additionally, the singlet state should have a lifetime long enough to facilitate the ISC to occur efficiently, yet not excessively long to avoid competing radiative or non-radiative decay pathways. Typically, the S_{1s} lifetime falls within the nanosecond range.[32] A sufficiently large singlet–triplet energy gap and a prolonged S_{1s} lifetime help to effectively promote ISC, ensuring a higher population of sensitizers in the triplet state necessary for subsequent energy transfer processes in the UCS.[23] In TTA-UC systems sensitized with semiconductor nanocrystals, the high spin–orbit coupling induces mixing between orbitals and spin states. As a result, the first excited singlet state of the sensitizer exhibits singlet–triplet character, making the ISC process practically negligible, with a consequent removal of the Φ_{ISC} term from the Φ_{UC} equation:[23,33,34]

$$\Phi_{UC} = \Phi_{TET}\Phi_{TTA}\Phi_{F}f \quad (2)$$

For an efficient TET, the triplet state of the sensitizer (T_{1s}) should be more energetic than the triplet state of the annihilator (T_{1a}) to provide a thermodynamic driving force for the process to occur. However, studies have shown that UC can still occur even when T_{1a} is slightly higher than T_{1s}, likely due to the strong donor–acceptor coupling or other favorable dynamics.[35,36] However, a large driving force between the triplet state energies of the sensitizer and annihilator leads to a smaller anti-Stokes shift, resulting in a lower energy gain.[37] Therefore, when designing a TTA-UC system, a balance must be found between maximizing the driving force for an efficient TET and maintaining a sufficient anti-Stokes shift to ensure an effective UC emission. In particular, in the case of nanocrystal-sensitized TTA-UC, the Φ_{TET} calculation should also address the role of the ligands on the surface of the nanocrystal when they act as mediators between the sensitizer and the annihilator (Table 1). TET occurs through Dexter-like processes (*e.g.* Dexter energy transfer and uncorrelated charge transfer steps, Scheme 2),[25] which are exponentially suppressed with the increasing distance between the donor and acceptor. The triplet-excited state energy of the transmitter ligand should be between that of T_{1s} and T_{1a} to ensure the driving force for the electron transfer.[14] Several studies report that phenyl group-containing ligands tend to promote TET more efficiently compared to aliphatic chain-containing ligands.[33,62] Moreover, the passivation of the nanocrystal-surface with the shell of a higher band gap semiconductor seems to enhance the TET rate as will be explained below.[50,63]

Φ_{TTA} is determined by using the T_{1a} lifetime of the annihilator molecules and based on the probability of having intermolecular collisions between them, which is associated with their distance and diffusion capability in a dispersion; this can be affected by several factors like temperature, viscosity of the medium and chemical affinity with the annihilator.[64] In the case of a TTA-UC system embedded into a solid-state matrix, the formation of S_{1a} can occur either through intermolecular collision or, in the case of a dense hosting medium, through energy migration from one annihilator to the other one; this is influenced by the physico-chemical properties (crystallinity, electronic properties, *etc.*) of the hosting medium itself.[65]

Several competitive processes can negatively impact Φ_{TTA}, including non-radiative decay pathways such as intersystem crossing from T_{1a} back to the ground state, or the O_2-induced quenching effect, limiting the practical application of TTA-UC nanoparticles in direct contact with air.[66] However, a few studies have proposed methods to mitigate the O_2-induced quenching effect in TTA-UC systems.

One approach involves the use of an organic/inorganic shell coating,[67,68] which acts as a physical barrier, preventing oxygen from quenching the triplet states and therefore reducing the efficiency of the TTA process. Another strategy used a molecular engineering approach by designing both the sensitizer and the annihilator with triplet states at lower energies than the singlet state of molecular oxygen. In this case, oxygen quenching can be minimized, allowing UC to proceed more efficiently even in the presence of air (see Section 4.3 below).[69–72]

The rate of TTA is also influenced by the intensity of incident light (Fig. 1b).[23] Below a certain intensity threshold (I_{th}), typically ranging from a few hundred mW cm^{-2} to several W cm^{-2}, non-radiative processes, such as ISC or triplet quenching, tend to outcompete the TTA process. In this low-power range (known as the "weak regime"), the upconverted emission intensity has a quadratic relationship with the incident light power. Instead, when the excitation power exceeds I_{th}, the TTA process becomes dominant over non-radiative pathways. In this "strong" regime, the upconverted emission transitions to a linear dependence on the incident light power, resulting in a more efficient and intense photon output.[61,73]

The f term is influenced by the electronic density of states of the annihilator. When two triplet states annihilate, the process can result in the formation of a higher-energy singlet state,

Table 1 A comprehensive overview of the main families of transmitter ligands used in nanocrystal-based triplet–triplet annihilation upconversion systems[a]

Ligand	Category	Type of ligands	Main characteristics	NCs	Ref.
PAH	Naphtalene based	NCA	Good TET efficiency and a triplet energy level at around 2.6 eV	$CsPbBr_3$ and CdS	38 and 39
	Acene-based	9-ACA, 9-ADTC, 9-EA, 9-VA, 2-ACA, 5-TCA, 5-CT, 5-CPT, 5-CPPT, 2,3-PyAn, PyP#PAn	Low-lying triplet states and long triplet lifetimes; energy levels can be tuned by varying the conjugation and adding functional groups	CdSe, CdSe/ZnS, InP/ZnSe/ZnS, ZnSe/InP/ZnS, $CuInS_2$/ZnS, Zn-$CuInSe_2$, InAs/ZnSe, PbS, PbS/CdS, CdTe, Si, and $CsPbBr_3$	14, 33, 40–52
	Pyrene-based	1-PCA	Good stability	$CsPbBr_3$, Ce-$CsPbBr_3$, and $CsPbX_3$ (X = Br/I)	49, 53, 54
	Phenanthrene based	3-PTCA; 9-PTCA	Good TET_1 efficiency	CdS and CsPbBr3	38 and 55
Derived or NO PAH		10-Ph-ADP	High binding affinity on the surface and higher TET	CdSe	56
		BA		CdS	38
		BCA	Facile anchoring on the surface	CdS and ZnSe/ZnS	38 and 57
		PPO	High stability and flexible molecular design	CdS/ZnS	58
		Rhodamine B		$CsPbBr_3$ and CdSe/ZnS	59 and 60
		Th-DPP	Easy synthesis and functionalization, inexpensive, and photostable	PbS	61

[a] Abbreviations: PAH: polycyclic aromatic hydrocarbon; NCA: 1-naphthoic acid; ACA: anthracence-carboxylic acid; ADTC: anthracene dithiocarbamate; EA: ethylanthracene; VA: vinylanthracene; TCA: tetracene carboxylic acid; CT: carboxylic acid tetracene; 4-CPT: 5-(tetracen-5-yl) benzoic acid; 5-CPPT: 4-(tetracen-5-yl)-[1,1-biphen2,3-biphenyl]-4-carboxylic acid; PyAn: bis-pyridine anthracene; PyP#Pan: modified anthracene with a pyridine anchoring group and *p*-oligophenylene; PCA: 1-pyrenecarboxylic acid; PTCA: phenanthrene-carboxylic acid; 10-Ph-ADP: 10-phenyl-anthracene dihydrogen phosphate; BA: benzoic acid; BCA: 4-biphenylcarboxylic acid; PPO: 2,5-diphenyloxazole; Th-DPP: thiophene-substituted diketopyrrolopyrrole.

a higher-energy triplet state, or even a quintet state. The likelihood of producing each of these states depends on the type, orientations and interaction nature of the two annihilators.[37,73]

The fluorescence QY (Φ_F, or PLQY) of the emitter (when present) needs to be as close as possible to one. It can be reduced by several competitive non-radiative processes, including intra- or intermolecular charge transfer, and vibrational or rotational decays. To maximize Φ_F, and thus enhance UC efficiency, the design of the emitter structure as well as its environment should be carefully selected.[74]

2.2. Criteria for the selection of the sensitizer

Unlike lanthanide-based UC systems, which typically rely on a determined sensitizer–emitter pair (with Yb^{3+} as the sensitizer and Er^{3+}, Ho^{3+}, and/or Tm^{3+} as emitters), TTA-UC offers greater flexibility. This is achieved by finely tuning the desired optoelectronic properties through a careful design of the sensitizer-annihilator chromophore structures, such as selecting the appropriate metal center and ligand in metal–organic complexes or optimizing the size, composition, defectivity and hybrid core–shell structure in NCs. To choose a suited photosensitizer in order to maximize Φ_{eff}, these criteria should be satisfied: (1) a high solubility in the hosting solvent and in a liquid medium, or a high degree of dispersion in the hosting matrix, when the UC system is embedded in a solid; (2) a high extinction coefficient at the incident radiation frequencies; (3) for organic/organometallic dyes as the sensitizer, a high tendency to promote ISC to generate a high number of triplet states; (4) an energy band-gap between singlet and triplet states comparable to the annihilator's one; (5) a long-living triplet state, for efficient triplet energy transfer to the annihilator; (6) for NCs as the sensitizer, a sufficiently high energy difference (typically higher than 0.2 eV) between T_{1s} and the triplet excited state of ligands (T_{1L}) anchored to the NC surface, acting as TET mediators between the sensitizer and annihilator (Scheme 3).[13,75] Considering these key criteria, organic sensitizers have been extensively explored due to their well-defined photophysical properties. In the following section, we briefly discuss the main classes of organic sensitizers, highlighting their advantages and limitations. However, since this review focuses primarily on NC-based sensitizers, which possess unique features that require further exploration, these will be examined in detail in Section 3.

2.2.1. Organic sensitizers. In the early 60s, the first sensitizers for delayed fluorescence (UC process) used by Parker and Hatchard were phenanthrene and proflavine hydrochloride molecules in ethanol, coupled with naphthalene and anthracene to convert UV and short visible light, respectively.[1]

Only recently, advances in the synthesis of heavy metal–organic complexes provided a breakthrough. Many of these

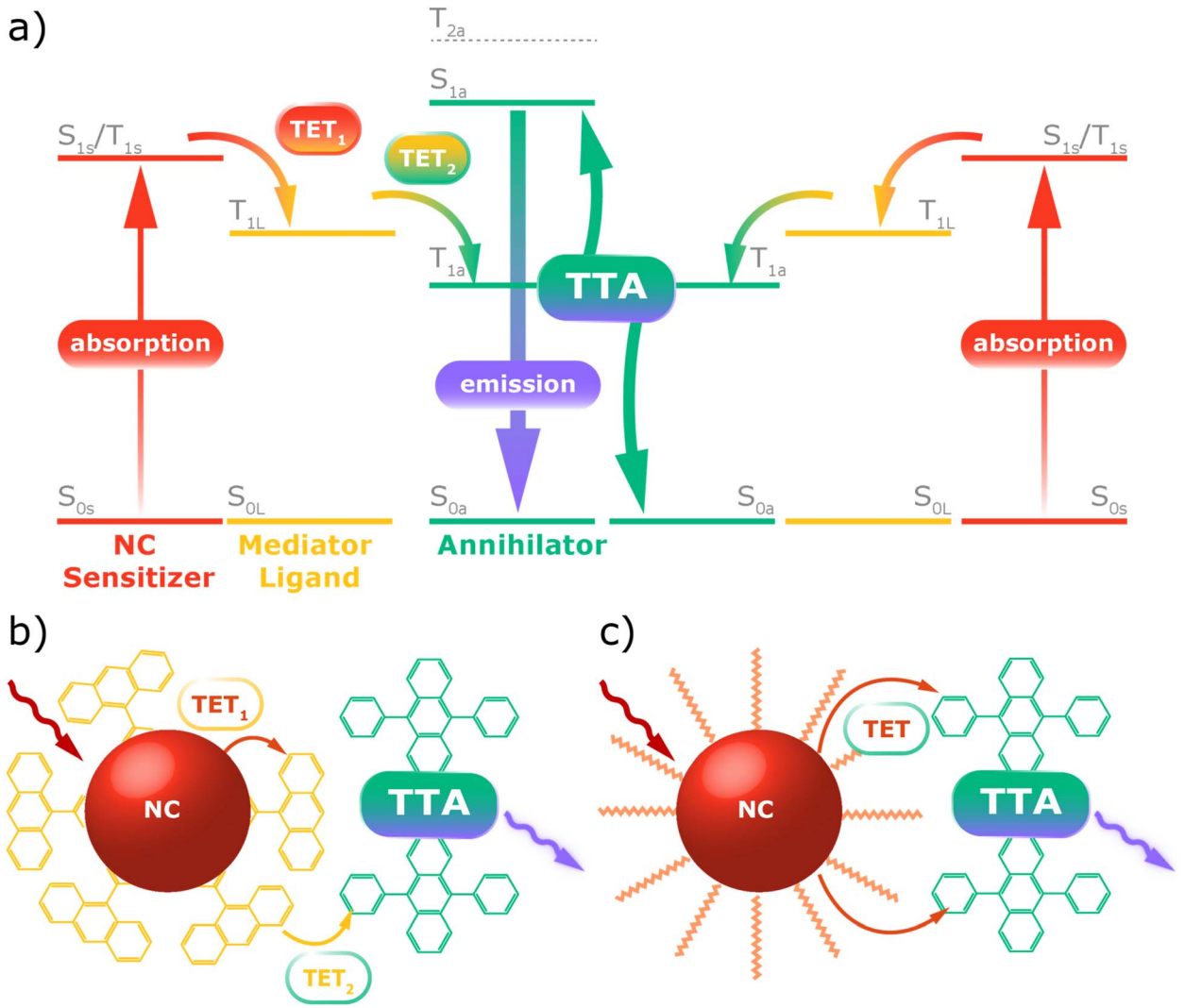

Scheme 3 (a) Jablonski diagram demonstrating NC-sensitized TTA-UC. Note that in this case ISC is absent, whereas in the presence of a ligand mediator TET is achieved by the contribution of TET_1 and TET_2. (b) Scheme showing TET processes from the NC to the mediator (TET_1) and from the mediator to the annihilator (TET_2), or (c) in the case of the absence of the mediating species, directly from the NC to the annihilator.

complexes exhibited stable, long-lived triplet states at room temperature, paving the way for TTA-UC to emerge as a dynamic and rapidly growing area of research.

Porphyrins, particularly Pt(II)-porphyrins and their analogues, are among the most extensively studied sensitizers for the UC process due to their absorption properties and good stability compared to most other organic dyes, relying on a planar macrocyclic ligand structure to prevent metal ion dissociation. They remain stable under mild oxidizing conditions, in the presence of reducing agents, in solvents with extreme pH values, and at elevated temperatures (~200 °C or beyond).[71,76] Other widely used classes of metal–organic compounds employed as TTA-UC photosensitizers generally contain metal centers such as Pd(II), Ru(II), Re(I), and Ir(III), paired with ligands like phthalocyanine, polyimine, and cyclometalated complexes.[13,76] The inclusion of a heavy-metal ion guarantees a high ISC efficiency.[77–79] For instance, one of the highest UC quantum yields of 27% was achieved by Nishimura *et al.*[28] in solution, using a TTA-UC system with PdTPBP as the sensitizer and TIPS-Ac as the annihilator. This system successfully converted long-wavelength visible light (λ_{UC} = 785 nm) into shorter-wavelength visible light, producing an anti-Stokes shift of 1.03 eV.

Metal-free organic compounds have also been developed as photosensitizers, carefully designed to optimize ISC and TET efficiencies for an effective TTA-sensitizing performance. These compounds include fullerene dyads, boron-dipyrromethene derivative (BODIPY) dyes, fluorophores with heavy-atom substitutions, bromine- and fluorine-substituted chromophores, biacetyl derivatives, and photo-switchable sensitizer pairs.[80–82]

Organic and organometallic photosensitizers developed so far can absorb radiation across a broad wavelength range, from blue through the entire visible spectrum and into the beginning of near-infrared (NIR).[83] UC emission generated by TTA with

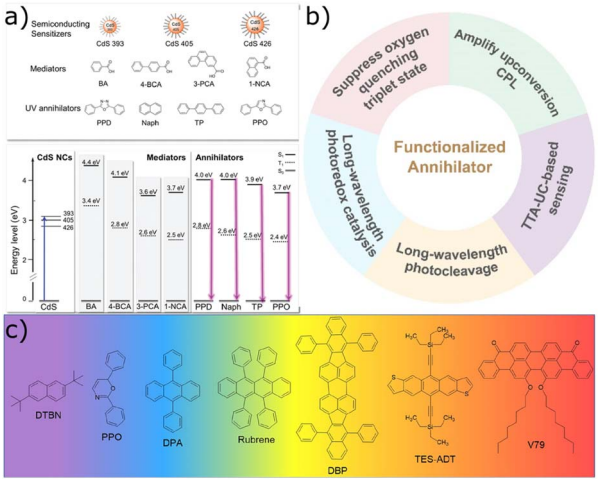

Fig. 2 (a) Illustration of semiconductor nanocrystal CdS along with the molecular structures of the four mediators and the four UV annihilators—PPD, Naph, TP, and PPO. The diagram depicting the energy levels of the CdS nanocrystals, mediators, and UV annihilators is given below. Reproduced from ref. 38 with permission from Wiley-VCH GmbH, Copyright 2021; (b) applications of functionalized annihilators. Reproduced from ref. 85 with permission from AIP Publishing, Copyright 2024; (c) chemical structures of the most used annihilator in the presence of NCs as the sensitizer. Reproduced from ref. 75 with permission from John Wiley & Sons Australia, Copyright 2024.

these photosensitizers spans from deep red to near-ultraviolet (NUV), reaching wavelengths of approximately 360 nm.[68,84]

2.3. Criteria for the selection of the annihilator

The annihilator choice is also substantial (Fig. 2a). To maximize Φ_{eff}, it should accommodate some criteria: (1) its energy levels should not allow the absorption of incident light; (2) the T_{1a} should have proper energy, namely lower than the one of the sensitizer (T_{1s}) but higher than half the energy of the singlet state of the emitting annihilator (S_a), allowing efficient TET and TTA processes; (3) it should have a sufficiently long lifetime in order to effectively ensure the TTA phenomenon; (4) it should be able to radiatively emit the photon coming from the singlet exciton, providing a high photoluminescence QY or, for some applications like photocatalysis, it could also provide efficient charge/exciton transfer to the active species/catalytic centers.[68,86–88] Annihilators normally serve as emitters but, recently, their chemical functionalization has broadened their role, which should be taken into consideration for their selection (Fig. 2b): they can be obtained as organic gels to prevent triplet quenching from oxygen, enhance the asymmetry factor of circularly polarized luminescence, act as recognition units in (bio)sensors, function as photocages for the controlled release of target molecules (especially BODIPY, perylene and anthracene derivatives),[85] and serve as photocatalysts[87] for low energy-driven organic transformations (see Scheme 4 below, Section 4.1).

Annihilators generally consist of polycyclic aromatic hydrocarbons (PAHs) with condensed benzene rings, as well as certain heterocyclic compounds. In particular, anthracene and tetracene derivatives are the most involved species for this purpose. Among these, especially in NC-sensitized TTA-UC systems (Fig. 2c), DPA, for UC from green to blue light, and rubrene, for NIR to yellow UC, are particularly targeted, thanks to their high singlet-radiative emission QY (namely, 97% in cyclohexane and 98%, in toluene, respectively).[13,75,89–91]

Hou *et al.*[38] combined three sizes of CdS nanocrystals (NCs) with four mediators and four annihilators (5-diphenyl-1,3,4-oxadiazole, naphthalene, *p*-terphenyl, and 2,5-diphenyloxazole), and achieved upconverted emission near 4 eV (from visible to UV light). The highest Φ_{UC} of 10.4% and the lowest threshold intensity (I_{th}) of 0.95 W cm^{-2} were obtained using 3.5 nm CdS NCs, phenanthrene-3-carboxylic acid (3-PTCA) as the mediator, and 2,5-diphenyloxazole (PPO) as the annihilator under 405 nm excitation (Fig. 2a). Their findings highlight some key design principles for optimizing NC-based TTA-UC, such as ensuring that the mediator's triplet level is at least 200 meV below that of the NC and selecting annihilators with similar triplet levels to the mediator for enhanced efficiency. Also, to preserve the surface from defectivity and maximize energy transfer efficiency, the mediator ligands were just added into solutions, without additional washing steps, typical of a classic ligand exchange procedure.[38]

The number of compounds exploited as annihilators has been slowly increasing. For instance, Qi *et al.*[92] investigated the opto-electronic response of a new annihilator species, namely π-expanded diketopyrrolopyrrole (π-DPP), coupled with palladium tetraaryltetranaphthoporphyrin (PdTNP) as the sensitizer, dispersed in a polystyrene matrix, for NIR-to-visible TTA-UC.[75]

Unlike other conventional annihilators, π-DPP does not generate reactive oxygen species (ROS) through electron transfer, preventing the formation of superoxide anions and singlet oxygen-induced degradation. As a result, π-DPP exhibits superior resistance to photobleaching and a significantly higher photostability over time.

In another study,[93] the successful triplet sensitization of 1-chloro-9,10-bis(phenylethynyl)anthracene (1-CBPEA) shows the possibility to overcome the limitation of rubrene as the sole compatible annihilator for solid-state perovskite-sensitized photon UC. In a recent study, using bulk perovskite as the sensitizer,[5] Sullivan *et al.*[94] investigated naphtho [2,3-*a*]pyrene (NaPy) as an annihilator in both solution-based and solid state based TTA-UC systems. Their findings showed that the higher aggregation and organization degree of the NaPy molecules let to a decrease in the S_a energy into a higher TET rate from the sensitizer-based film, resulting in a higher upconverted emission from the aggregated singlet state and weak emission from the higher lying singlet state. Chua *et al.*[53] showed the synergy effect of simultaneously using two annihilators, DPA and TIPS-An, which has led to a fivefold increase in upconversion efficiency compared to the linear sum of the individual systems. They proposed that the increase in UC efficiency could be attributed to an energy resonance between the sum of the triplet excited states of both annihilators and the singlet excited state of DPA.[53] These studies highlight the ongoing efforts to expand the range of viable annihilators for both solution-based and solid-state TTA-UC systems, paving the way for improved efficiency and broader applicability, which are further discussed in

Section 4. Building on this foundation, the following section delves into TTA-UC systems sensitized with nanocrystals, exploring their unique advantages and challenges in comparison to more traditional sensitizers.

3. TTA-UC systems sensitized with nanocrystals

Semiconductor-NCs, also known as quantum dots (QDs), are luminescent materials with nanometric dimensions, featuring opto-electronic properties that lie between those of bulky materials and single molecules.[95]

They are an excellent demonstration of the quantum confinement effect in matter, initially observed at the beginning of the 80s by Ekimov and Efros in a glassy matrix,[95] and by Brus in a colloidal medium.[96] Since their discovery, QDs attracted a lot of interest in several fields, from opto-electronic devices to bio- and energy applications.[97–100] In photocatalysis, QDs have been utilized in various photo-induced reactions, such as the reduction of CO_2 into value-added chemicals (*e.g.*, CO, CH_3OH, CH_4, and HCOOH) and the production of H_2 either alone or coupled with another substrate/catalyst.[101–104]

Currently research is moving toward low-toxicity QDs, such as InP, $CuInS_2$, $CuInSe_2$, or $AgGaSe_2$. These QDs are being explored as viable alternatives to the more widely studied Pb- and Cd-based NCs, characterized by their exceptional opto-electronic properties, but low sustainability.[105] In the last decade,[106] a new class of semiconductor NCs, inorganic metal halide perovskite, (initially in the form of colloidal lead halide perovskite, LHP) has also emerged showing a size-dependent optical bandgap, unique optoelectronic features and a non-linear process (*e.g.* MEG).[107,108] Since their discovery, this field has seen tremendous progress in synthesis methods, ligand engineering and potential applications such as in quantum light[109] sources and photocatalysis.[110]

Recently, semiconductor NCs have also found applications as photosensitizers for TTA-UC. In the first study on the subject, Huang *et al.*[111] used PbSe and CdSe QDs as sensitizers coupled with rubrene and DPA as emitters, to convert NIR light (980 nm) into yellow light (568 nm) and green light (532 nm) into blue light (432 nm), respectively (Fig. 3a). In such systems, octadecyl phosphonic acid and 9-anthracene carboxylic acid (9-ACA) were used as mediator ligands. In the 9-ACA-CdSe/DPA system, an anthracene-based ligand, able to transfer energy from the nanocrystal to the emitter, resulted in a marked enhancement of Φ_{TET}, leading to a three orders of magnitude increase in Φ_{UC}.

One year later, Wu *et al.*[112] reported a solid-state NC-sensitized TTA-UC from $\lambda > 1$ μm to visible emission, using colloidal PbS QDs as sensitizers, capped with oleic acid ligands, deposited onto a 80 nm layer of rubrene doped with 0.5% vol of dibenzotetraphenylperiflanthene (DBP) as the host/guest annihilator/emitter system (Fig. 3b).

In a few years, Φ_{eff} of TTA-UC systems synthesized by using QDs has increased from 0.01% to more than 20% thanks to an engineered control of NC structures by (i) partial replacement of the native capping ligands (*e.g.* oleic acids) with transmitter ligands (*e.g.* tetracene mediators); (ii) formation of a core/shell structure to suppress harmful charge-transfer from QDs to the transmitter ligand; (iii) high-purity of the QD precursors to increase the exciton lifetime.[37,50,113,114] Through these optimizations, Gray *et al.*[58] first reported a Φ_{UC} of 2.6% with CdS/ZnS core–shell QDs from 405 nm to 355 nm. The Φ_{UC} was later enhanced up to 5.1% by He *et al.*,[39] who employed $CsPbBr_3$ perovskite QDs, whereas Han *et al.*[51] reported that surface-anchored core/shell 9-ACA $CuInS_2$/ZnS with DPA as the annihilator showed a Φ_{UC} of 9.3%. Very recently, Sun *et al.*[40] reported the use of InAs/ZnSe QDs with 5-carboxylic acid tetracene (5-CT) as the mediator which was able to efficiently sensitize rubrene to upconvert red light (at 808 nm) into orange light (with an emission intensity at 570 nm), with an excellent Φ_{UC} (Table 2). These remarkable improvements in the Φ_{UC} highlight the crucial role of rational NC design and surface engineering. Among these strategies, the use of capping ligands (Scheme 3) as energy transfer transmitters between NC-sensitizers and annihilators has proven to be a key factor, as discussed in the following section.

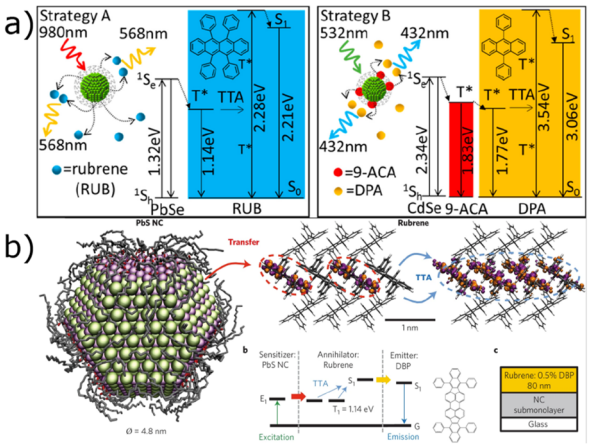

Fig. 3 Pioneering studies for TTA-UC sensitized with NCs (a) in a liquid medium. Reproduced from ref. 111 with permission from American Chemical Society, Copyright 2015; (b) in the solid state. Reproduced from ref. 112 with permission from Springer Nature, Copyright 2016.

3.1. The role of transmitter ligand

The implementation of capping ligands (Scheme 3) as energy transfer mediators between NC-sensitizers and organic annihilators significantly enhances the quantum efficiency of the system and eqn (2) becomes

$$\Phi_{UC} = \Phi_{TET}\Phi_{TTA}\Phi_F f = \Phi_{TET_1}\Phi_{TET_2}\Phi_{TTA}\Phi_F f \quad (3)$$

where Φ_{TET_1} is the energy transfer efficiency from the sensitizer to the mediator ligand and Φ_{TET_2} is the energy transfer efficiency from the mediator ligand to the annihilator (Fig. 4a).[41,137] To demonstrate their versatility in efficiently promoting energy transfer to the emitter, Huang *et al.*[111] investigated additional conjugated species as mediators beyond 9-ACA, including octadecyl phosphonic acid (ODPA), 2-ACA, and 1-ACA, since

Table 2 Summary of the most relevant TTA-UC systems sensitized with semiconductor nanocrystals (NCs) and molecular dyes. Since TTA-UC is a two-photon process, Φ_{UC} values are reported accordingly. Only TTA-UC systems with $\Phi_{UC} \geq 0.5\%$ have been included, highlighting those with the highest upconversion performance. The upconversion emission wavelength (λ_{em}) and anti-Stokes shifts (ΔE_{AS}) are listed based on the most intense UC signal[a]

Sensitizer	Mediator	Annihilator	λ_{exc} (nm)	λ_{em} (nm)	Φ_{UC} (%)	ΔE_{AS} (eV)	I_{th} (W cm^{-2})	State	Ref.
NC sensitizer									
CdSe (2.7 nm)	9-ACA	DPA	532	~430	3.85	0.55	—	Liquid	115
CdSe (2.6 nm)	9-ACA	DPA	532	432	7.15	0.54	—	Liquid	113
CdSe (2.6 nm)	CPA	DPA	532	432	1.95	0.54	—	Liquid	113
CdSe (~2.4 nm)	9-ACA	DPA	532	~430	5.95	~0.55	—	Liquid	42
CdSe (2.4 nm)	2,3-PyAn	DPA	532	432	6.05	0.54	0.15	Liquid	116
CdSe/ZnS (~3.05 nm)	9-ACA	DPA	488	430	4.65	0.34	—	Liquid	45
CdSe/ZnS (6.1 nm)	RhB	DPA	635	~402	1.4	~1.13	0.55	Liquid	60
CdSe (~1.9 nm)	9-ACA	DPA	532	430	8.0	0.55	0.574	Liquid	117
Au doped CdSe (2.3 nm)	9-ACA	DPA	532	440	~12	0.49	0.2	Liquid	118
CdSe (2.4 nm)	PyP0PAn	DPA	488	430	5.8	0.34	—	Liquid	33
CdSe (2.4 nm)	PyP1PAn	DPA	488	430	2.25	0.34	—	Liquid	33
CdSe (2.4 nm)	10-Ph-ADP	DPA	488	430	8.5	0.56	0.163	Liquid	56
CdSe (2.3 nm)	9-ACA	DPA	532	430	~1.5	0.55	10	Solid	119
CdS/ZnS (4.8 nm)	PPO	PPO	405	355	2.6	0.43	7.1	Liquid	58
CdS (3.5 nm)	3-PTCA	PPO	405	~365	10.4	~0.33	0.95	Liquid	38
CdTe NR (3 nm × ~10 nm)	9-ACA	DPA	520	~425	4.3	0.53	0.093	Liquid	43
PbS/CdS (~3.4 nm)	5-CT	Rubrene	808	560	4.2	~0.68	0.0032	Liquid	120
PbS/CdS (3.2 nm)	5-CT	Rubrene	785	560	2.5	0.63	—	Liquid	50
PbS (~4.8 nm)	—	Rubrene-0.5% DBP	808	612	~0.61	0.50	—	Solid	112
PbS (~2.5 nm)	HA	Rubrene-0.5% DBP	808	610	3.5	0.50	—	Solid	34
PbS-S (2.7 nm)	5-CT	Rubrene	781	560	2.3	0.63	—	Liquid	121
PbS-T (2.7 nm)	5-CT	Rubrene	781	560	5.9	0.63	53.4	Liquid	121
PbS (2.73 nm)	Th-DPP	Rubrene	808	~580	6.75	~0.6	4.8	Liquid	61
$CuInS_2$/ZnS(2.5 nm)	9-ACA	DPA	520	400	9.3	0.72	~4.7	Liquid	51
Zn doped $CuInSe_2$/ZnS (4 nm)	5-TCA	Rubrene	808	~560	8.35	~0.7	2.1	Liquid	14
InP/ZnS/ZnSe (~3.1 nm)	9-ACA	DPA	530	402	5.0	0.74	0.57	Liquid	46
ZnSe/ZnS (~4.4 nm)	BCA	DTBN	405	321	3.1	0.80	2.4	Liquid	57
ZnSe/InP (4.6 nm)	9-ACA	DPA	532	~460	4.16	~0.36	1.2	Liquid	47
ZnSe/InP-ZnS (5.8 nm)	9-ACA	DPA	532	~460	4.00	~0.36	0.6	Liquid	47
InAs/ZnSe (~2.8 nm)	5-CT	Rubrene	808	570	10.5	0.64	~20.2	Liquid	40
Si (3.1 nm)	9-EA	DPA	488	~430	3.5	0.34	0.95	Liquid	48
Si (3.1 nm)	9-EA	DPA	488	432	~8.59	0.33	—	Liquid	122
Si (3.1 nm)	9-VA	DPA	485	~430	1.8	~0.33	0.5	Liquid	44
Si (3.1 nm)	9-VA	tBu$_4$P	532	~490	8.6	~0.28	0.5	Liquid	44
$CsPb(Br/I)_3$ (9.1 nm)	NCA	PPO	445	363	>2	0.63	4.7	Liquid	123
$CsPbBr_3$ (~3.5 nm)	NCA	PPO	443	355	5.1	0.69	1.9	Liquid	39
$CsPbBr_3$ (3.2 nm)	2-ACA	DPA	443	~400	6.5	~0.3	6.9	Liquid	49
$CsPbBr_3$ (~4 nm)	RhB	DPA	447	~400	3.55	0.33	~0.7	Liquid	59
$CsPbBr_3$ (9 nm)	RhB	DPA	447	~400	0.7	~0.33	~1	Liquid	59
$CsPbBr_3$ (4.5 nm)	9-PTCA	PPO	473	355	2.25	~0.87	~2.2	Liquid	55
Ce-$CsPbBr_3$ (~6 nm)	PCA	DPA	450	~440	2.4	0.06	—	Liquid	54
Organic sensitizer									
Ru-4		DPA	473	~430	4.8	~0.26	—	Liquid	124
PtOEP		DPA	532	435	26	0.52	0.0006	Liquid	125
PtOEP		AAB-DPA	532	440	30	0.49	0.009	Liquid	69
PtOEP		DPA	532	440	1.0	0.49	0.53	Solid	126
PtOEP		DPAS	532	445	23.8	0.46	0.034	Solid	127
PdBrTPP		DPA	532	~436	~17.1	~0.51	—	Liquid	128
PtTPTNP		Rubrene	690	560	3.3	0.42	—	Liquid	129
PtTPTNP		PDI	690	580	3.0	0.34	—	Liquid	129
PtTPBP		BPEA	635	~470	15.5	~0.69	0.2	Liquid	130
PdTPBP		TIPS-Ac	635	430	27	0.93	0.9	Liquid	28
ZnTPPOH		TTBPer	532	~460	12.25	~0.36	0.359	Solid	131
Ir-3		DPA	473	~400	14.05	~0.47	—	Liquid	132
$Ir(C6)_2$(acac)		1,4-TIPS-Nph	445	372	10.25	0.55	0.0023	Liquid	133

Table 2 (*Contd.*)

Sensitizer	Mediator	Annihilator	λ_{exc} (nm)	λ_{em} (nm)	Φ_{UC} (%)	ΔE_{AS} (eV)	I_{th} (W cm^{-2})	State	Ref.
NC sensitizer									
$Ir(ppy)_3$		2,7-DTBP	447	376	4.8	0.52	—	Liquid	134
BDP-F		9-PEA	650	432	1.55	0.96	0.0196	Liquid	135
4CzBN		1,4-TIPS-Nph	405	~370	16.8	0.29	0.297	Liquid	136

[a] Abbreviations: AAB-DPA: amphiphilic acceptor based DPA; BDP-F: iodized BODIPY dimer; BPEA: 9,10-bisphenylethynylanthracene;CPA: (4-(anthracen-9-yl)benzoic acid); DPAS: sulfonate anion grafted DPA; DTBN: 2,6-di-*tert*-butylnaphthalene; HA: hexanoic acid $Ir(C6)_2(acac)$: Ir coumarin acetylacetone complex; $Ir(ppy)_3$: Ir (2-phenylpyridine)$_3$ complex; Ir-3: cyclometalated Ir complex; NR: nanorod; PbS-S/T: PbS NCs, synthesized with bis(trimethylsilyl)sulfide/thiourea sulfur precursors, respectively; PdBrTPP: Pd tetrabromophenylporphyrin; PDI: perylenediimide; PdTPBP: Pd *meso*-tetraphenyltetrabenzoporphine complex; PtOEP: Pt octaethyl-porphyrin; PtTPTNP: Pt tetraphenyltetranaphthoporphyrin; RhB: rhodamine B; Ru-4: ruthenium polyimine complex; ^{t}Bu4P: 2,5,8,11-tetra-*tert*-butylperylene; TIPS-Ac: 9,10-bis[[(triisopropyl)silyl)ethynyl]anthracene; TTBPer: 2,5,8,11-tetra-*tert*-butylperylene; 1,4-TIPS-Nph: 1,4-bis((triisopropylsilyl)ethynyl) naphthalene; 2,7-DTBP: 2,7-di-*tert*-butylpyrene 4CzBN: 2,3,5,6-tetra(9*H*-carbazol-9-yl)benzonitrile; 5-CT: 5-carboxylic acid tetracene; 9-PEA: 9-phenylacetylene anthracene; PPOS: 4-(2-phenyloxazol-5-yl)benzenesulfonate; ZnTPPOH :zinc complex of 2-{3-[10,15,20-tris(3,5-di-tert-butylphenyl)- porphyrin-5-yl]phenoxy}ethanol.

Φ_{TET} is determined either based on the positions of the triplet energy levels of the three species to promote a cascade process, or based on the length and the nature of the ligand. In particular, since triplet electrons are transferred through a Dexter-like process, the overlapping between triplet wavefunctions of the three moieties is fundamental (Scheme 3).[23] The strong exponential dependence between the TET rate constant (k_{TET}) and the distance between the donor and the acceptor (d), in the case of a Dexter process, can be described by using:[33,113,138]

$$k_{TET} = k_0 e^{-\beta d} \quad (4)$$

where k_0 is the TET rate constant when the distance between the donor and the acceptor is null and β is the attenuation factor, related to the nature of the energy barrier between the donor and the acceptor (please note that the donor and acceptor change according to the considered TET). A higher β value indicates weaker coupling, which results in a reduced energy transfer rate. This value is influenced by the energy offset between the donor and acceptor, the tunneling barrier, and the length of the bridging units.[33] For instance, with a mediator, β is larger for aliphatic ligands, compared to phenylene-based ones, due to the higher energy barrier (Fig. 4b).[137] With the use of a transmitter ligand, a careful design of the energy cascade within the system is required to achieve efficient TTA-UC as a multi-step energy transfer often results in significant energy losses. Therefore, several key factors must be considered before choosing a mediator ligand, such as alignment of energy levels, binding affinity, and stability, as suggested by Tang's group.[33,139]

The triplet energy levels of the transmitter ligand should be carefully positioned: lower than the NC donor's dark excitonic state to provide a thermodynamic driving force, yet higher than the acceptor's triplet state. This energy offset, which influences the TET rate, can be adjusted by modifying the NC size: a larger offset typically enhances energy transfer efficiency. Moreover, the excited electronic states in the mediator ligand should predominantly decay through radiative pathways (*i.e.*, high PLQY). Non radiative decays, excimer formation and quenching phenomena between close transmitters can be avoided by increasing the symmetry of the molecule and introducing bulky groups (Fig. 4c).[113,139] To ensure efficient energy transfer, the ligand should also bind strongly to the NC surface. L-type ligands (*e.g.*, amines, pyridines, and phosphine oxides) typically bind less strongly and more reversibly to the surface than anionic X-type ligands (*e.g.*, carboxylates, thiolates, and phosphonates) while multidentate ligands can also strengthen bonding to NCs. Additionally, the binding group should also preserve the NC's photoinduced excitonic states and avoid charge transfer, which make thiols, in some cases, not the preferred choice.[139] In perovskite NCs, both carboxylate and alkylammonium ligands can dynamically attach to the surfaces, which facilitate the exchange of native ligands with carboxylate-functionalized naphthalene ligands (*e.g.* deprotonated 1-naphthalenecarboxylic acid, 1-NCA).[39]

The choice of the group anchored to the sensitizer NC influences β as well (Fig. 4d). For instance, the substitution of pyridine with a carboxyl attaching group in CdSe-(phenylene)$_n$-DPA caused an increase in β from 0.43 A^{-1} to 0.72 A^{-1}, which is detrimental for k_{TET}.[33,113] To reduce energy losses and ensure compliance with energy conservation principles, the triplet energy of the annihilator should be nearly equal to that of the transmitter, while its singlet state energy should be slightly lower than but close to twice the triplet energy.[139]

The ligand should also be stable in time. Generally, the energy transfer from the nanocrystal (donor) to the ligand mediator (acceptor) follows a Dexter mechanism. Huang *et al.*[33] designed a transmitter ligand formed by three main moieties: a pyridine anchoring group, an anthracene moiety as the triplet energy acceptor and a *p*-oligophenylene bridge as the spacer to control the distance from the donor (NC) to the acceptor (anthracene).

The transition from short-range tunneling to long-range hopping can be controlled by increasing the bridge length (Fig. 4e and f). This finding suggests that for longer distances (>1 nm) hopping is the preferred mechanism and it has weak

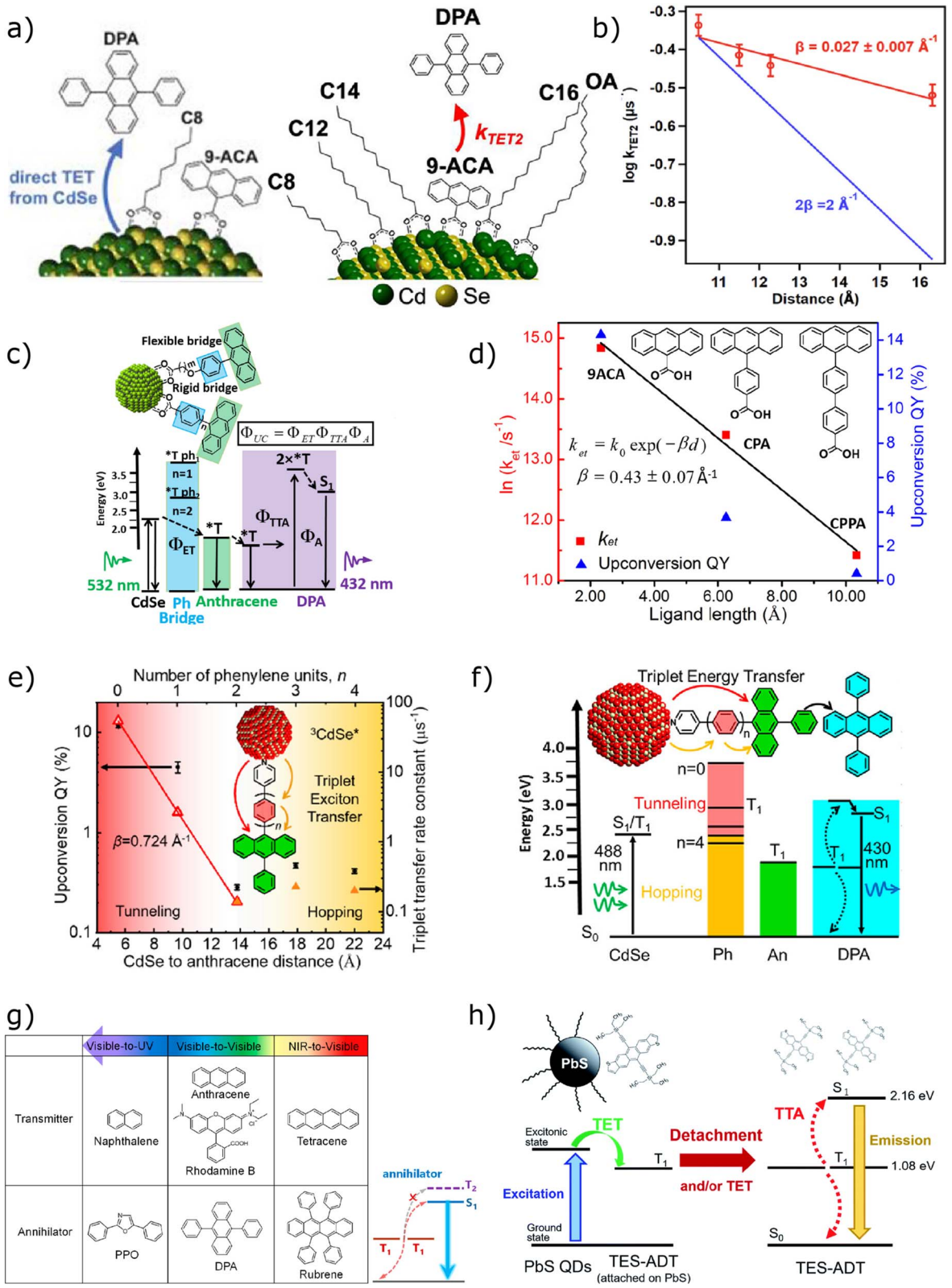

Fig. 4 (a) Schematic representation of TET from the CdSe QD surface in the absence of a mediator ligand and when the QD surface is capped with carboxylic acid ligands of varying lengths to the 9-ACA transmitter ligand (TET_1), followed by subsequent transfer from 9-ACA to the DPA emitter (TET_2); reprinted with permission from ref. 137 Copyright 2022 American Chemical Society. (b) Exponential fit of the rate of TET_2 (k_{TET_2}) *vs.* the carboxylic acid ligand length with the damping coefficient; reprinted with permission from ref. 137. Copyright 2022 American Chemical Society; (c) diagram that illustrates the triplet excitonic states of the CdSe NCs, the *p*-phenylene (ph) bridge for $n = 1$ and 2, and the anthracene transmitter;[113] (d) plots of the k_{TET} and maximum Φ_{eff} (red squares and blue triangles, respectively) *vs.* the phenylene bridge length in the anthracene transmitter ligands;[113] (e) Φ_{eff} and TET *vs.* the number of phenylene bridge showing the switch from a tunneling process to a hopping

distance dependence. Recently, Miyashita *et al.* showed that oligoyne bridges enable energy transfer across greater distances while preserving a rapid rate of transfer, particularly in comparison to traditional phenylene-based molecular bridges.[140] In another study, they also reported that aliphatic ligands with more than 8 carbon atoms significantly hamper triplet energy transfer, while shorter ligands, like octanoic acid, enable direct energy transfer from CdSe QDs to DPA emitters, achieving a remarkable Φ_{eff} of 6.9% without a transmitter ligand.[137]

Reducing the length of ligands on the NC surface has been shown to accelerate TET rates from the NC to acceptor molecules. However, excessively short ligands can saturate the transfer rate and introduce defects, ultimately lowering the quantum yield. Therefore, the optimal ligand length should strike a balance between enhancing the TET rate, preserving colloidal stability, and avoiding defect formation.[34,141]

Functionalized polycyclic aromatic hydrocarbons (PAHs) are frequently used as ligands due to their favourable triplet energy levels and good stability (Table 1).[25] These molecules, including acene,[115] pyrene[54] and naphthalene[123]-based ligands often exhibit significant singlet–triplet energy splitting, providing triplet energies suitable for their role as acceptors (Fig. 4g).[25,54,115,123] However, their high singlet energy levels can sometimes hinder singlet energy transfer from NCs. The rigid molecular structures of PAHs also contribute to their effectiveness by extending triplet lifetimes and reducing energy loss through torsional or rotational motions. This makes them particularly suitable as transmitters in NC-sensitized systems across different energy conversion ranges, including visible-to-UV and visible-to-visible UC applications.

Other classes of ligands have also been explored, such as oligothiophene carboxylic derivatives,[142] phenyl-linked aromatic compounds,[57] oxazole based compounds,[143] as well as modified PAH based ligands.[42]

The introduction of mediator ligands might create three main drawbacks in the TTA process: (i) an energy loss (>200 meV), (ii) a limited ability to accept energy in the NIR region, and (iii) the formation of surface-localized states after ligand exchange with a slowed down energy transfer from the NC to the bound ligand, particularly for acene-type ligands.[139,144] Nishimura *et al.*[74] addressed some of these issues by coupling 5,11-bis(triethylsilylethynyl)anthradithiophene (TES-ADT) with PbS nanoparticles (Fig. 4h). The thiophene group in TES-ADT facilitated binding to the PbS surface while also allowing for convenient detachment after the TET_1 process. Such a dual functionality enabled TES-ADT to act as either a mediator or an annihilator. These hybrid nanomaterials successfully converted NIR light at 1064 nm into orange visible light (with an emission peak at approximately 600 nm), achieving an anti-Stokes shift of about 0.9 eV. However, the UC efficiency was limited due to the short triplet lifetime and low triplet energy transfer (TET) driving force exhibited by the sensitizers with only $\Phi_{UC} = 0.047\%$.[74]

Jiang *et al.* recently showed that thiophene-substituted diketopyrrolopyrrole (Th-DPP) weakly interacts with lead cations on the PbS surface, promoting the electronic coupling between the NC and the ligand triplet exciton transfer and bringing the efficiency close to 100% even with a small energy gap (0.04 eV).[61]

3.2. Shape and composition of NCs

For more efficient NC-sensitized TTA-UC systems, besides engineering the ligand, it is possible to change the NC composition, size and morphology. For example, Au doping in CdSe can reduce nonradiative hole-transfer to the ligand highest occupied molecular orbital with a consequent increase in TET_1 (Fig. 5a).[118] Similarly, Liang *et al.*[14] demonstrated that Zn doping, up to a certain threshold, significantly enhances the photosensitizing properties of $CuInSe_2$, increasing the final Φ_{UC} fourfold, from 2.4% to 8.35% compared to that of the undoped system (Fig. 5b).

In perovskite QDs the TET, and consequently the TTA, was increased by incorporating Ce^{3+} ions increasing the Φ_{UC} from 0.85% to 2.40%.[54] It was also noted that the Φ_{eff} is directly correlated with the NC QY and inversely correlated with the size of NCs due to the quantum effect of particle size on bandgap energy, which influences the energy transfer driving force from the NC-sensitizer to ligands.[115] Mahboub *et al.* demonstrated a dramatic improvement in upconverted light intensity with smaller NC sizes. For PbS NCs, reducing the size from 3.5 to 2.9 nm resulted in a 700-fold enhancement, while for PbSe NCs, a size reduction from 3.2 to 2.5 nm led to a 250-fold increase.[146] A similar trend was observed in Cd based QDs as well (Fig. 5c).[115,119]

In $CsPbBr_3$ NC–pyrene complexes, the TET efficiency increased from nearly zero in bulk-like NCs to ~99% in strongly confined NCs, as quantum confinement enhances the energy transfer by increasing electronic coupling between NCs and acceptors through higher carrier probability densities at the NC surfaces.[147]

The optical quality of the QD sensitizer is a crucial parameter to achieve high upconversion efficiency. To enhance the quantum yield and stability and decrease the surface traps, shelling the quantum dots with another semiconductor having a similar lattice structure to minimize mismatch and interface defects is a common technique. The shell allows obtaining different heterostructures, such as type I or type II, based on the band alignment between the core semiconductor and the shell semiconductor (Fig. 5d).[46,63] Type I core/shell structures are

process. Reprinted with permission from ref. 33. Copyright 2020 American Chemical Society; (f) schematic to illustrate the ET process in CdSe NC sensitized UC, where yellow arrows stand for triplet exciton hopping and red arrows for tunneling; reprinted with permission from ref. 33. Copyright 2020 American Chemical Society; (g) principal structures of representative transmitter and annihilator molecules used in NC-sensitized TTA-UC systems. The diagram on the right illustrates the ideal electronic configuration for an efficient annihilator. Reprinted with permission from ref. 25. Copyright 2021 American Chemical Society. (h) Sketch to show the TES-ADT ligand dynamics in PbS QDs for the UC process; reproduced from ref. 74 with permission from Royal Society of Chemistry, Copyright 2019.

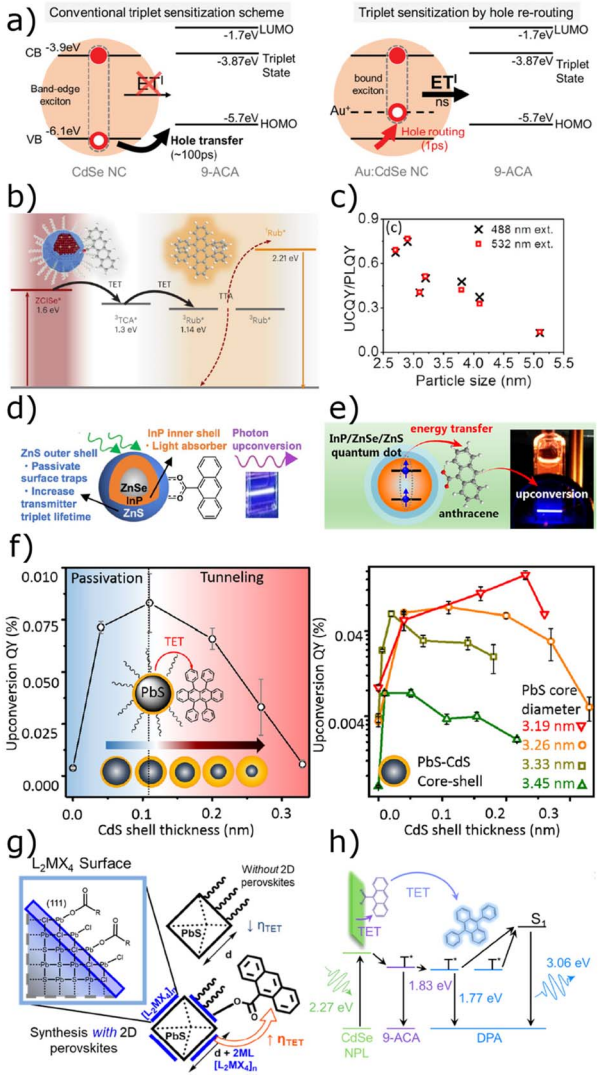

Fig. 5 (a) Schematic of the energy mechanism in undoped and Au-doped CdSe; reprinted with permission from ref. 118. Copyright 2020 Wiley-VCH GmbH. (b) Schematic of the TTA system synthesized by using zinc doped ZnS shelled $CuInSe_2$ (ZCISe); reprinted with permission from ref. 14. Copyright 2023 Springer Nature; (c) Φ_{eff} normalized for the PLQY *vs.* particle size; reprinted with permission from ref. 115 Copyright 2015 American Chemical Society; (d) inverse type-I ZnSe/InP/ZnS core/shell/shell as the sensitizer for TTA from NIR to blue light; reprinted with permission from ref. 47. Copyright 2023 American Chemical Society; (e) double shelled type I InP/ZnSe/ZnS as the sensitizer for TTA from green to blue light; reprinted with permission from ref. 46. Copyright 2020 American Chemical Society; (f) Φ_{eff} *vs.* CdS shell thickness in PbS QDs based on different PbS core sizes; reproduced from ref. 120 with permission from American Chemical Society, Copyright 2016; (g) 2D perovskite shelling on PbS QDs; reprinted with permission from ref. 145 Copyright 2024 American Chemical Society. (h) CdSe nanoplatelets as the TTA sensitizer. Reprinted with permission from ref. 117. Copyright 2020 American Chemical Society.

often employed for triplet sensitization, where the wide-bandgap shell confines the exciton to the core and passivates surface ions, suppressing nonradiative decay.

The shell thickness is critical due to its dual role: while it passivates traps to enhance PLQY and energy transfer efficiency, it also acts as a tunneling barrier that can hinder TET between the NC core and mediators/annihilators as Dexter-type TET is highly distance-sensitive.[75] Optimizing the shell thickness involves balancing these effects. For instance, a thin shell improves PLQY and UC efficiency, while a thicker shell reduces wave function overlap between the donor and acceptor by slowing the energy transfer. Additionally, minimizing the energetic mismatch between the core and shell can lower the damping coefficient for Dexter energy transfer, facilitating more efficient ET.[148]

Various NC systems illustrate the impact of shell engineering on TTA-UC, especially in Cd-based-ZnSe and InP used as the core in visible-to-visible or UV range UC processes. For example, a 4 layer ZnS shell on CdS NCs increased the PLQY from 4.4% to 26% and the TET efficiency to 90%, achieving a Φ_{UC} of 2.6%.[58]

In visible light TTA-UC, CdSe/ZnS NCs are one of the most studied host/guest heterostructures.[75] It achieved an optimized Φ_{UC} of 4.6% with a 1.5-monolayer ZnS shell, while with a CdS shell, the core/shell system showed reduced performance due to shorter exciton lifetimes and exciton–phonon coupling.[45] Similarly, ZnSe NCs with a 1.4 monolayer ZnS shell achieved a high PLQY of 78% and a Φ_{UC} of 3.1% due to balanced defect passivation and TET efficiency.[57]

Double shelled type I InP/ZnSe/ZnS QDs capped with 9-ACA ligands were used as the sensitizer to convert green (530 nm) to blue light (402 nm) with a Φ_{UC} of 5% (Fig. 5e).[46] An inverse type I heterostructure was applied to convert NIR light into visible light (Fig. 5d). In ZnSe/InP core/shell NCs with two monolayers of ZnS for a final structure ZnSe/InP/ZnS, the InP inner shell was used to absorb light and the outer ZnS to passivate surface traps and to increase the transmitter's triplet lifetime, although it does not increase the final Φ_{eff}.[47]

In the NIR range, in PbS NCs, CdS monolayer shells or ZnS sub-angstrom thick shells significantly improved Φ_{eff} by suppressing competitive charge transfer, especially for the holes, and extended triplet lifetimes (Fig. 5e).[50,120,149] For instance Huang *et al.*[50] by encapsulating PbS QDs in a CdS shell coupled them with a tetracene ligand and rubrene emitter, to increase Φ_{UC} from 1.75% to 2.5%. Imperiale *et al.*[145] showed that a 2D perovskite shell in ultrasmall PbS nanocrystals (with diameter <2 nm) enhances photoluminescence efficiency by reducing surface-mediated nonradiative losses and exciton–phonon coupling (Fig. 5f). This improved passivation leads to longer excited-state lifetimes and higher triplet yields, making these nanocrystals more effective as sensitizers in upconversion.

Usually the core/shell QDs show a spherical/cubic shape with 3D quantum confinement and isotropic optoelectronic features. Anisotropic properties can be provided by changing the morphology and quantum confinement in 1D (*e.g.* nanorods, nanowires, and nanotubes) or in 2D (*e.g.* nanoplatelets and nanosheets) (Fig. 5g) either of the entire heterostructure or the shell alone. Both Cd based nanorods and nanoplates showed a promising lower power threshold compared to similar spherical QD systems and yet, a still low efficiency (*e.g.* Φ_{UC} = 4.3% and 2.7%, respectively), suggesting that further improvements are required.[43,117]

The ability to engineer both the surface and morphology of QDs to tailor their optical properties makes them ideal sensitizers. The following sections explore different classes of QDs, from well-established to more recently developed ones.

3.3. Classes of QDs

3.3.1. Traditional II–VI, III–V and IV–VI group QDs. CdSe, PbS, PbSe, CdTe, InAs, and GaAs QDs were among the first NCs synthesized exhibiting quantum size effects. Over the years, their synthesis methods have been optimized to achieve high photoluminescence quantum yield, enhanced optical and environmental stability, and versatile surface functionalization through heterostructures or ligand replacement. For these reasons, they are widely employed in various optical devices as well as photovoltaics and photocatalysis.[150]

In the classic II–VI and III–V semiconductor nanocrystals, the conduction band is mainly characterized by cation s-type orbitals whereas the valence band consists mainly of anion p-type orbitals. With this configuration, electrons show a well-defined spin quantum number ($S = 1/2$), while holes are characterized by a total angular momentum quantum number $J = 1/2$ or $J = 3/2$.[25]

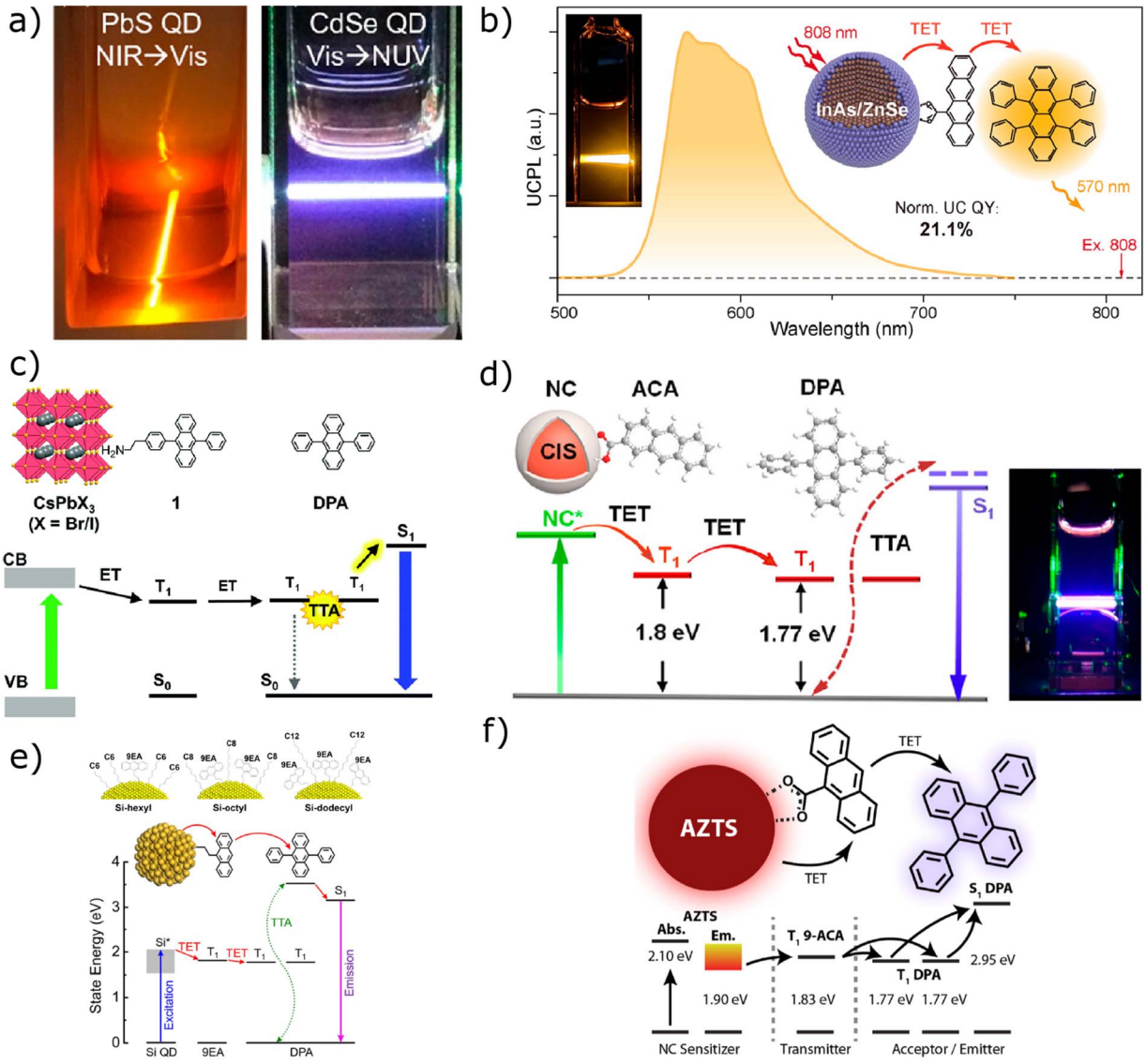

Fig. 6 (a) Photographs of TTA-UC from NIR to visible and from vis to NUV by applying PbSQDs and CdSe QDs as sensitizers, respectively. Reproduced from ref. 37 with permission from American Chemical Society, Copyright 2024; (b) TTA scheme for InAs/ZnSe-5CT and rubrene. Reproduced from ref. 40 with permission from American Chemical Society, Copyright 2024; (c) TTA scheme using $CsPbX_3$ perovskite QDs as the sensitizer. Reproduced from ref. 151 with permission from Royal Society of Chemistry, Copyright 2017; (d) TTA scheme for $CuInS_2$/ZnS-ACA with a DPA system and photograph of the upconverted light. Reproduced from ref. 51 with permission from American Chemical Society, Copyright 2019; (e) TTA system with Si QDs as the sensitizer, functionalized with 9 EA as the mediator ligand and alkyl chain ligands to maintain solubility and the energy diagram of the system. Reproduced from ref. 122 with permission from Royal Society of Chemistry, Copyright 2022; (f) TTA system with pirquitasite Ag_2ZnSnS_4 QDs as the sensitizer. Reproduced from ref. 152 with permission from American Chemical Society, Copyright 2024.

At ambient temperature, bright and dark excitons in semiconductor NCs are under thermal equilibrium due to weak bright-dark exciton splitting caused by strong electric field screening and large Wannier exciton size. This small splitting (<20 meV), one or two orders of magnitude lower than the singlet-triplet splitting in molecules (hundreds of meV to ~1 eV), on the one hand, makes energy loss due to ISC virtually negligible (its yield can be omitted, as reported in eqn (2); on the other hand, it shortens the exciton lifetime. Such a significantly shorter lifetime, compared to that of molecule-based triplet sensitizers, has important implications for designing NC-sensitized TTA-UC systems (Fig. 6a). Cd chalcogenides are among the most widely utilized NCs for sensitization applications. To the best of our knowledge, the highest reported Φ_{eff} for NC-sensitized TTA-UC was achieved by Ronchi *et al.*[118] (Fig. 5a). In their study, they employed Au-doped CdSe NCs as sensitizers, functionalized with 9-ACA ligand/mediator species, and coupled them with a DPA emitter. Upon irradiation with a 532 nm laser, the TTA-UC system exhibited a blue upconverted emission centered at 440 nm, achieving an impressive Φ_{UC} of approximately 12% (Table 2).

Pb chalcogenide QDs can extend their optical properties also in the NIR, beyond 1100 nm, providing, in theory, extremely high anti-Stokes shifts.[74,153] Similarly, as already mentioned, InAs/ZnSe core–shell QDs have been proven to be highly effective NIR sensitizers, achieving one of the highest Φ_{UC} values ever reported for NC-sensitized TTA-UC (10.5%) (Fig. 6b).[40]

3.3.2. Pb-based perovskite QDs. Another emerging class of semiconductor NCs that can be efficiently applied as sensitizers thanks to their exceptional electronic properties are lead-halide perovskite QDs, with the general formula ABX_3 (where A is a monovalent cation, B is the Pb(II) ion, and X is a halide anion). These NCs exhibit extremely high absorption cross-section in the UV and visible ranges, a highly tunable bandgap, low exciton binding energy, and exceptionally strong radiative emissions. Perovskite opto-electronic features can also be tuned by properly changing A, B or X components, or by doping, having a cubic crystal structure, which can be distorted into orthorhombic or tetragonal structures with a low activation energy.[54,154] This newly emerging class of NCs, lead- or tin-based perovskites, show an "inverted band structure", *i.e.*, holes in the valence band possess a defined spin state, while electrons in the conduction band, influenced by a spin–orbit coupling, are defined by a total angular momentum $J = 1/2$.[25,155]

The first study utilizing perovskite QDs as UC sensitizers was conducted by Mase *et al.*[151] in 2017, where $CsPbBr_3$ perovskite NCs were coupled with DPA, achieving 434 nm UC emission from 532 nm excitation with an $\Phi_{UC} = 0.65\%$, as reported in Fig. 6c. Three years later, He *et al.*[49] significantly improved the efficiency, reaching a remarkable Φ_{UC} of 6.5% by employing $CsPbBr_3$ NCs capped with 2-ACA mediators and paired with DPA. Most of the studies are limited to blue-to-UV upconversion, due to the lack of suitable transmitters and emitters from green-to-UV. While the Φ_{eff} (0.014%) remains much lower than that of blue-to-UV systems, the first successful green-to-UV TTA-UC was achieved by introducing a sulfonated PPOS transmitter that effectively receives triplet energy from green-light-absorbing LHP NCs and passes it to TIPS-Nph as the emitter with low triplet energy and strong UV fluorescence.[143] Mixed halide perovskite nanocrystals ($CsPbX_3$, X = Br/I) have also been used as the sensitizer in a composite system[53] to demonstrate the synergy effect between two annihilators, as already mentioned in Section 2.3. Chakkamalayath *et al.*[156] provided detailed insights into the kinetics and mechanisms of multistep energy transfer in the LHP NC sensitized TTA system with rubrene–DBP (annihilator–emitter), especially in the film state. Triplet transfer from $CsPbI_3$ to rubrene occurs with 70% efficiency and a rate constant of 9×10^8 s^{-1}. The rubrene triplets undergo TTA, producing delayed fluorescence lasting up to 10 μs, far longer than its intrinsic 15 ns lifetime. The DBP emitter then captures this energy (94% energy transfer efficiency),[157] leading to upconverted emission.

However, the drawbacks displayed by these nanomaterials, like their poor chemical stability, low absorption coefficient in the NIR, Pb-related toxicity, and short exciton lifetimes, lead to some limitations in their applicability in this field so far.[158]

3.3.3. Environmentally friendly QDs. In the last few decades, driven by increasing environmental awareness and the desire to expand the use of QDs, significant efforts in the field of NC semiconductors have focused on the synthesis and study of non-toxic QDs. These efforts have particularly targeted binary II–VI, III–V and IV–VI, single-element IV and ternary I–III–VI QDs.[159]

Ternary I–III–VI QDs. Ternary I–III–VI QDs, such as $CuInS_2$ (CIS), $CuInSe_2$, $AgInS_2$, $AgInSe_2$, $CuGaS_2$, and $AgGaSe_2$, exhibit unique opto-electronic properties.[160,161] These include a size-dependent bandgap, enabled by their strong quantum confinement effect, which allows precise tuning of their spectral response from the visible to the NIR range. Coupled with their low toxicity and good sustainability, these features position them as promising alternatives to traditional binary QDs for a wide range of applications, such as in solar energy conversion, photocatalysis, light-emitting devices (LEDs), photodetectors, and bioimaging.[162]

Owing to their ternary composition, these systems exhibit a higher concentration of point defects and a broader size distribution, compared to traditional binary QDs. These factors account for their extended photoluminescence lifetimes (in the range of hundreds of nanoseconds, which is an order of magnitude higher than that of conventional binary QDs), their pronounced Stokes shifts as well as their wide absorption and emission bands.[159,163] Notably, the relatively low enthalpy of formation for point defects, combined with the high mobility of group I ions, may contribute to the significant defect concentrations observed in these systems, resulting in non-stoichiometric structures, leading to numerous trap levels within the band-gap. The sustainability of these NCs and their synthesis routes, together with their unique opto-electronic properties, like their high absorption coefficient over a wide energy range and their relatively long exciton lifetimes (compared to Cd and Pb based QDs), made I–III–VI QDs very promising as TTA-UC photosensitizers.[164] In particular, CIS QDs are good candidates thanks to their direct band-gap, their high extinction coefficient in the yellow-to-red range and their high defect tolerance and

photo/chemical stability.[159] For instance Han *et al.*[51] in their work managed, by coupling CIS NCs with a ZnS shell (CIS/ZnS) capped with anthracene (ACA) ligands to a DPA annihilator, to obtain green-to-violet UC emission (Fig. 6d). They attributed the higher exciton lifetime displayed by these sensitizers (~200 ns) to the hole trapping induced by Cu-point defects, which contributed to obtain a remarkable $\Phi_{UC} = 9.3\%$. However, the exciton "self-trapping" process also resulted in a non-negligible energy loss with the consequence of a weaker anti-Stokes shift, compared to the one displayed by traditional II–VI, III–V and IV–VI QD-sensitized TTA-UC systems. A thick shell, such as ZnS on CIS QDs as well as the introduction of Ga in the CIS structure can help to increase the PLQY and narrow the PL peak.[161] Additionally, doping and surface engineering are effective strategies to optimize performance.[160,165]

Other NCs with low/no toxicity. Over the past decade, in addition to ternary I–III–VI QDs, other environmentally friendly NCs have been explored as TTA-UC sensitizers, especially IV group-based QDs. Among these, Si-based QDs have drawn particular interest.

Being non-toxic and abundant, Si is an excellent choice for sustainable semiconductor NCs (Fig. 6e).[122] However, the covalent bonding nature and tetrahedral structure make the synthesis of Si-based nanoparticles different from the methods typically used for metal-based QDs.

Common synthesis approaches include non-thermal plasma treatments, chemical or electrochemical etching, and the reduction of silicon halides.[166] For instance Xia *et al.*[48] achieved upconversion of 488 nm to 425 nm light by coupling a DPA emitter with 9-ethylanthracene (9-EA) and octadecene (ODE) capped Si NCs, synthesized *via* the non-thermal plasma method. This system showed a Φ_{UC} of approximately 3.5%.

Wang *et al.*[44] achieved one of the highest UC yields, obtaining green-to-blue UC emission with $\Phi_{UC} = 8.6\%$ by coupling 3.1 nm Si QDs, mediated by 9-VA ligands, with $^{t}Bu_4P$ annihilators. However, similarly to ternary I–III–VI QDs, Si-based QDs also present some drawbacks related to exciton-energy losses, and the exact mechanisms governing their emission (*e.g.* indirect excitations or surface states)[46] remain a subject of debate.[25]

Another sustainable alternative is the use of non/less-toxic elements containing III–V QDs, such as InP based QDs. Characterized by a large excitonic Bohr radius (larger than the one associated with traditional II–VI, III–V and IV–VI group QDs, ~10 nm), high carrier mobility, and good absorption/emission properties (particularly in the deep red and in the NIR regions), these NCs have shown great potential as TTA-UC sensitizers, especially in light emitting devices.[167] Furthermore, a very recent advancement in more sustainable nanocrystals capable of driving photochemically relevant upconversion with a significant anti-Stokes shift includes the use of low toxicity quaternary Ag_2ZnSnS_4 (AZTS) QDs developed by Villanueva *et al.* (Fig. 6f).[152] Functionalized with triplet-extracting 9-ACA ligands and combined with molecular DPA annihilator/emitters in solution, these hybrid systems successfully converted red light ($\lambda_{ex} = 637$ nm) into blue light ($\lambda_{UC,PL} \sim 425$ nm).[152] Compared to conventional QDs, the synthesis, passivation, and surface engineering of these more environmentally friendly NCs still require further refinement. However, recent advancements in machine learning and artificial intelligence (AI) have demonstrated significant potential in accelerating this optimization process, for example to improve the monodispersity and optical properties of colloidal PbS QDs.[168] As these AI-driven approaches continue to evolve rapidly, they are expected to play a crucial role in overcoming current challenges, expediting the large-scale production of sustainable QDs, and fine-tuning their functional properties for different applications.

3.4. Comparison of nanocrystals and organic/organometallic dyes as sensitizers in TTA-UC systems

After having explored various classes of inorganic nanocrystals as triplet sensitizers, it is essential to compare their performance with that of traditional organic and organometallic dyes in TTA-UC systems. While nanocrystals offer advantages such as tunable optical properties, high absorption coefficients, and enhanced stability, organic and organometallic dyes have long been the dominant choice due to their well-defined triplet states and established functionalization strategies. However, the use of these organic sensitizers can lead to different challenges. The primary limitations of organometallic and organic dyes as photosensitizers include poor photostability, a limited responsiveness and inefficient energy conversion, caused by non-radiative decays and short triplet lifetimes, in the NIR range (especially beyond 1100 nm).[14,37,74] A significant challenge in all-organic TTA-UC systems arises from a high probability of overlapping absorption and emission bands between the sensitizer and annihilator, especially in the visible-to-near UV region, leading to reabsorption of upconverted photons by the sensitizer.[169] Additionally, the possibility of back energy transfer *via* the FRET mechanism to the sensitizer further decreases Φ_{eff}.[169] These issues coupled with the low sustainability displayed by these class of compounds, due to complex and long synthesis processes, pushed part of the scientific community to shift their attention to other possible classes of sensitizers for the TTA-UC process.[37,68]

Semiconductor QDs offer several advantages compared to molecular sensitizers: (1) their synthesis routes are generally scalable;[105] (2) their optical properties are easily tuneable from the visible to the NIR range by adjusting their size and shape;[148] (3) they have a high extinction coefficient, *i.e.* typically around one order of magnitude higher than that of organometallic/organic dyes, over a wide wavelength range (from the visible to the NIR);[71] (4) they generally show a higher PLQY.[170] Different from molecular sensitizers, semiconductor NCs are able to efficiently absorb more than one photon per-time (MEG, Scheme 1), which can consequently lead to a higher UC quantum yield.[37] (5) Due to the nature of triplet and singlet spin-mixed states there is practically no ISC step in QD-sensitized TTA-UC systems with the consequence of Φ_{ISC} omission from the members contributing to Φ_{UC},[23,33] (eqn (2)); (6) QDs generally display a higher photostability.[71] However, QDs also display certain weaknesses that can negatively impact their sensitizing properties, significantly affecting Φ_{eff}: (1) some are susceptible to oxygen-induced quenching;[171,172] (2) due to their small

splitting between bright and dark states, their exciton lifetimes generally are generally very short (on the order of nanoseconds), which is several orders of magnitude lower than those of molecular sensitizers;[25] (3) their high surface-to-volume ratio renders them highly reactive and prone to instability;[173] (4) surface defects act as trap states, reducing the number of charge carriers that are efficiently transferred.

To mitigate these issues, colloidal NCs are often coated with long-chain conjugated systems, polyaromatic compounds, or carboxylic acid-based ligands. However, these capping agents can interfere with the TET process, often necessitating the use of mediator ligands. Additionally, core/shell nanostructures can be engineered to enhance environmental stability or minimize surface defects, as discussed in previous sections. Optimizing NC-based sensitizers for efficient TTA-UC for practical applications remains an active area of research since it offers an exciting opportunity for harnessing low-energy photons in innovative ways. Building on these developments, the following section explores the diverse applications of TTA-UC systems (Fig. 7).

4. Applications

TTA-UC systems demonstrate notable potential in several diverse areas (Fig. 7), including photovoltaics, 3D printing, biology, biomedical applications and, more recently, photo-driven chemical reactions, such as photocatalysis and bond activation reactions, like photocaging, photocleavage and photoswitching.[30,67,87] In this review, photocatalysis is focused on, which stands to gain substantially from the adoption of these innovative light-converting systems.

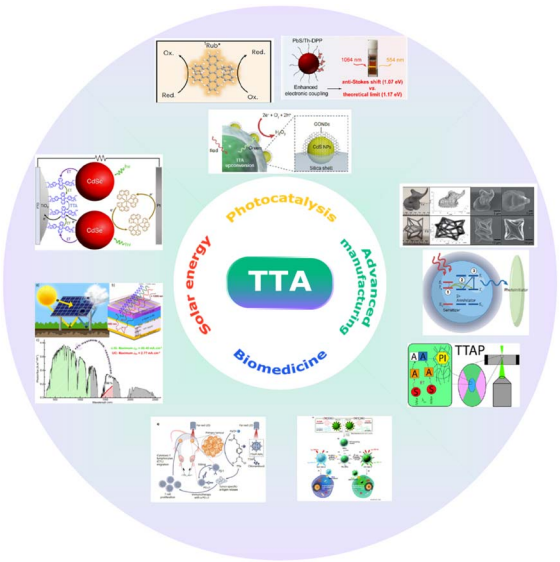

Fig. 7 Main fields of TTA applications, based on ref. 14, 61, 87 and 174–177. Reproduced from ref. 14 with permission from Springer Nature, Copyright 2023. Reproduced from ref. 61 with permission from American Chemical Society, Copyright 2024. Reproduced from ref. 87 with permission from Springer Nature, Copyright 2024. Reproduced from ref. 174 with permission from American Chemical Society, Copyright 2022. Reproduced from ref. 175 with permission from Elsevier, Copyright 2017. Reproduced from ref. 176 with permission from American Chemical Society, Copyright 2021. Reproduced from ref. 177 with permission from American Chemical Society, Copyright 2020.

4.1. Photocatalysis and photochemistry

Notoriously, a significant portion of the solar spectrum remains underutilized, as visible (~43%) and near-infrared (NIR) (~52%) photons, which make up the majority of the solar radiation at sea level, are inefficiently exploited. Low-energy photons can penetrate deeply into coloured solutions and biological tissues due to reduced scattering, but their low energy restricts their ability to drive many chemical transformations.[178,179]

TTA-UC may favour the exploitation of solar energy to drive several reactions of environmental and industrial interest, like H_2 evolution, CO_2 reduction, abatement of emerging contaminants, and synthesis of organic molecules and polymers.[37,68,87]

Multiphoton absorption-mediated photon UC has emerged as a promising solution, enabling the conversion of low-energy photons into higher-energy ones to enhance photochemical processes. Integrating TTA-UC nanocomposites with conventional semiconductor photocatalysts (*e.g.*, TiO_2, ZnO, g-C_3N_4, and MOFs) expands the usable solar spectrum, increasing electron–hole pair generation and improving reaction yields. Additionally, TTA-UC systems can operate efficiently under incoherent, low-intensity solar light while allowing flexible tuning of excitation and emission wavelengths. Coupling these upconversion systems with traditional photocatalysts, which primarily absorb UV photons (~5% of the total solar flux), offers a promising strategy for significantly enhancing solar energy utilization in photocatalytic applications.

In photo-driven reactions the use of lower energy photons offers further benefits: (i) higher probability of being absorbed by the photo harvesting antenna (*e.g.* TTA-UC system/photocatalyst) without competing with the reactant; (ii) reduction of undesired side reactions; (iii) higher penetration in different media, beneficial for both large-scale reactions and biological applications.[179]

Huang and Han[87] categorized the different photochemical processes based on the number of the involved components, namely three, two and single component. The three-component configuration (a sensitizer, an annihilator and a photocatalyst) is the general scheme for heterogeneous catalysis when a TTA-UC system sensitizes a traditional semiconductor, *e.g.* TiO_2 as proposed by Barawi *et al.*[180] (see Section 4.1.1 below). In a two-component configuration, where only the sensitizer and annihilator are present, the annihilator serves both as a triplet energy acceptor and as a photocatalyst, directly reacting with the target compound. For instance, tetra*tert*butylperylene (TTBP) functioned as both the annihilator and photocatalyst in the cyclization of dienyl azide to pyrroles (yield of 80%) upon UC of NIR light at 730 nm to blue light by the PtTPTNP sensitizer.[179]

In contrast, a single-component system, where the sensitizer alone has long triplet lifetimes and acts as both the annihilator and photoinitiator, is far less common. In such cases, the

photosensitizer can undergo TTA *via* Dexter energy transfer, particularly at high concentrations. This behavior has been observed mainly in the presence of Zn tetraphenylporphyrin (ZnTPP), where excited triplet states with twice the energy of the ground state exceed the energy of the corresponding higher excited singlet state. The latter state then directly serves as an electron donor, playing a key role in photochemical reactions by enabling inert bond activation and inducing, for instance, polymerization without requiring electron-sacrificial agents or photoinitiators.[87,181]

Based on the literature, the primary mechanisms of TTA-UC-assisted photo-driven reactions can be categorized into energy transfer processes and electron transfer processes. Energy transfer can occur either non-radiatively or *via* light emission (Scheme 4a). Considering the substrate as a conventional photocatalyst (*e.g.* in the three-component configuration) or a photoinitiator or the reactant itself (*e.g.* in the two-component scheme), the main processes are summarized in Scheme 4:[30,87] (1) radiative energy transfer: the electron in the singlet state decays to the ground state, leading to the emission of an upconverted photon, which is then absorbed by the substrate. (2) Non-radiative energy transfer: the electron–hole pair (exciton) from the singlet state of the emitter is transferred to the acceptor/substrate through Förster resonance energy transfer (FRET) or singlet-to-singlet Dexter energy transfer. (3) Single electron transfer: the electron, generated through the TTA process, is directly transferred to the acceptor and activates it. This mechanism is commonly observed in photoinduced redox processes.[134,182,183]

4.1.1. Photo(electro)catalytic H_2 production. Barawi *et al.*[180] were among the first to present a proof of concept study on photoinduced water electrolysis and H_2 evolution using upconverted photons (Fig. 8a). They designed a photoelectrochemical cell (PEC) consisting of a Pt cathode and a TiO_2 (anatase) based photoanode in contact with a colloidal solution of TTA-UC nanoparticles, where the sensitizer 2,3-butanedione (BA) was coupled with PPO as the emitter. Upon irradiation with a blue laser ($\lambda_{exc} = 445$ nm), the system exhibited upconversion (UC) emission, producing light with a 0.82 eV anti-Stokes shift and an emission band centered at 370 nm. The resulting UC UV light was absorbed by TiO_2 (Scheme 4b), generating electrons that were transferred to the Pt cathode, where they reduced water to H_2. Meanwhile, the photogenerated holes in TiO_2 were neutralized *via* oxidation of a sacrificial electron donor, namely sulfite ions (SO_3^{2-}), which were converted into sulfate ions (SO_4^{2-}).

Very recently, Madbak *et al.*[187] published a study on water splitting and H_2 evolution using a TTA-UC based photocatalyst. They integrated upconverting nanoparticles composed of $Ir(C6)_2(acac)$ as the sensitizer and a 1,4-TIPS-nph annihilator, into a UV-absorbing $Rh/Cr_2O_3/CoOOH/Al:SrTiO_3$ (Al:STO) photocatalyst. Upon irradiation with a visible LED light at 455 nm, the system emitted photons in the UV range (between 350 and 410 nm) with a Φ_{UC} ~6%, effectively matching the 3.2 eV band

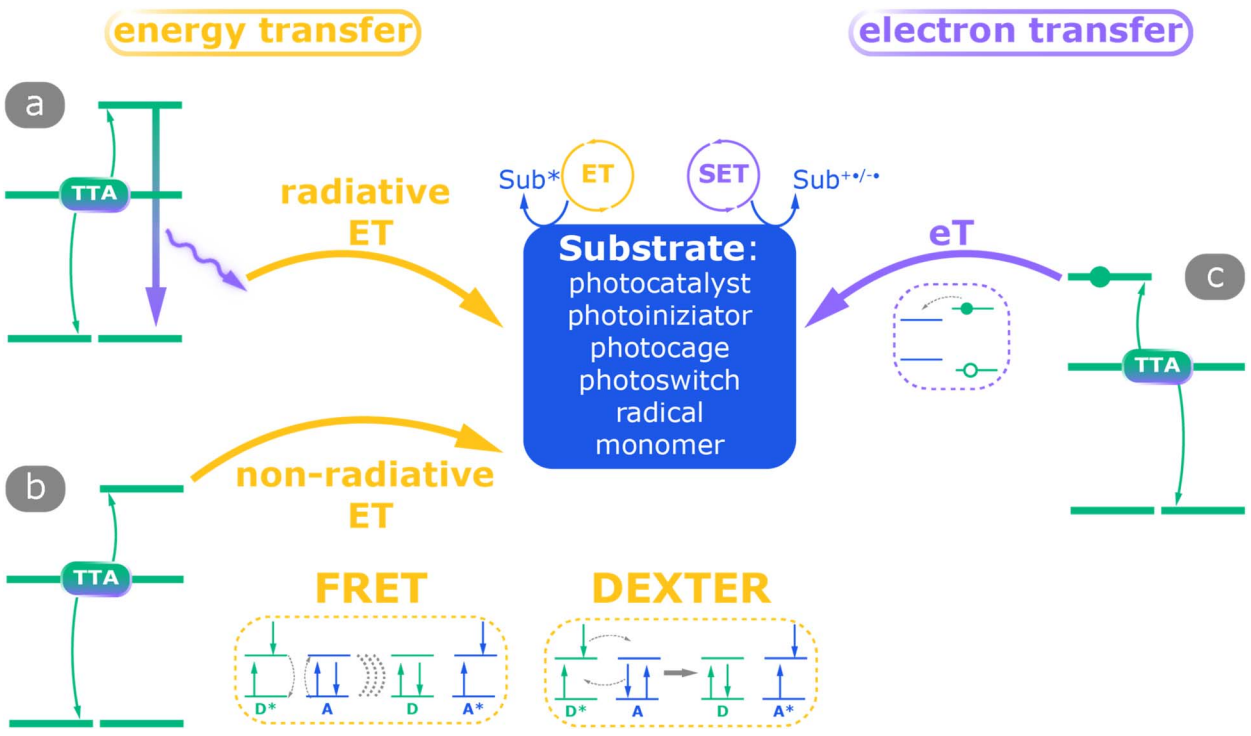

Scheme 4 Possible reaction mechanisms for TTA-UC mediated photochemical reactions.[30,87] The annihilator can serve either as an energy donor in energy transfer (ET) pathways or as an electron donor in the electron transfer pathway (eT). ET pathways include both a (a) radiative process and (b) non-radiative process, *e.g.* FRET and DEXTER mechanisms (in the insets D is the donor and A is the acceptor, and the asterisk indicates the excited state) whereas (c) in the eT pathway, the excited annihilator serves as the electron donor to the substrate.

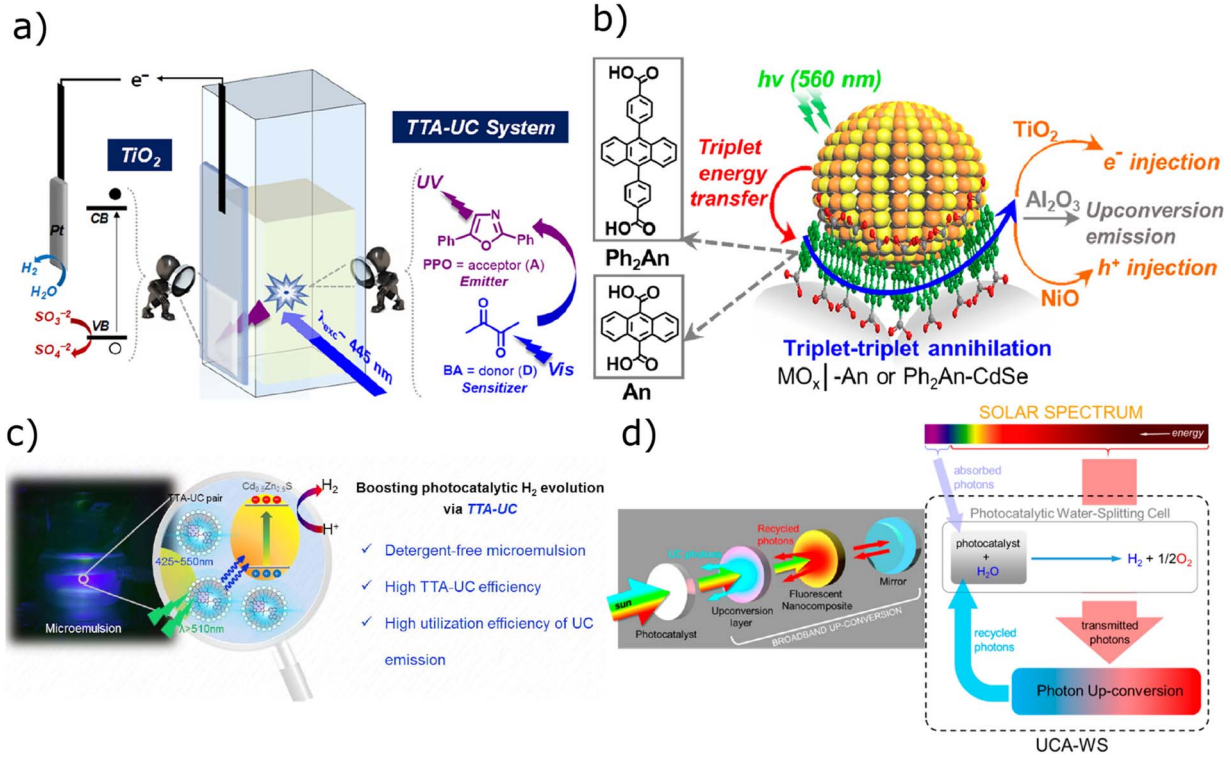

Fig. 8 H_2 photo(electro)catalytic production by applying TTA-UC based systems and devices. (a) Schematic illustration of a PEC sensitized by a TTA-UC system; reproduced from ref. 180 with permission from American Chemical Society, Copyright 2019; (b) schematic of the TTA-UC system to sensitize photoelectrodes; adapted from ref. 185 with permission from Elsevier, Copyright 2022; (c) schematic and photo of the microemulsion photocatalytic system; reproduced from ref. 184 with permission from American Chemical Society, Copyright 2019; (d) sketch of the architecture and concept of the TTA-UC water splitting device. Reproduced from ref. 186 with permission from American Chemical Society, Copyright 2017.

gap of the Al:STO photocatalyst and enabling H_2 evolution from water splitting. This study further demonstrated that integrating TTA-UC systems into a photocatalyst can enhance H_2 production by effectively utilizing visible light.[188] Oxide based photoelectrodes were sensitized by the TTA-UC process. These assemblies were composed of oleic acid-capped cadmium selenide (CdSe) nanocrystals, which were directly anchored onto a layer of surface-bound, carboxylic acid-functionalized anthracenes *via* ligand exchange. Upon green light excitation, these upconverting nanocrystal assemblies generated singlet excitons through sensitized triplet–triplet annihilation (TTA), which were efficiently injected into semiconductor electrodes, transferring electrons to the conduction band of TiO_2 (photoanode) and holes to the valence band of NiO (photocathode). By optimizing the interaction between surface-bound molecules and nanocrystals, the system enhances energy transfer and charge injection processes. These advancements could significantly improve photoelectrodes for applications in solar-driven water splitting and CO_2 reduction (Fig. 8b).[185]

The use of upconverting micelles is also a promising approach (Fig. 8c). For instance, PdTPBP-based compound as sensitizers coupled with an anthracene derivative (*e.g.* NBPEA)[189] or perylene[184] as acceptors were integrated into a micellar solution to boost H_2 production. This system upconverted red light into blue light, effectively sensitizing the $Cd_{0.5}Zn_{0.5}S$ catalyst. By extending the absorption range beyond 510 nm, surpassing the limitations of $Cd_{0.5}Zn_{0.5}S$ alone, the hybrid TTA photocatalytic system significantly enhanced hydrogen production. It achieved a hydrogen generation rate of 8.44 mmol g^{-1} h^{-1}, more than doubling the 4.04 mmol g^{-1} h^{-1} obtained with $Cd_{0.5}Zn_{0.5}S$ alone.[184] Another interesting method involves encapsulating TTA-UC clusters within a silica shell, which has been explored for sensitizing the g-C_3N_4-CdS heterostructured photosystem[190] for H_2 production and CdS/Pt photocatalyst[191] for both H_2 production and tetracycline (TC) degradation.

A photocatalytic heterostructure using the silica shell around the TTA-UC system in the presence of CdS QDs coupled with reduced graphene oxide (rGO) to enhance charge separation and to lower the recombination was also proposed by Chandrasekaran *et al.*[188]

Engineering strategies for photo-driven devices, such as the integration of upconversion layers, can also boost the overall system's photocatalytic performance. Monguzzi *et al.*[186] developed an upconversion-enhanced photoelectrochemical (PEC) water-splitting system to improve solar energy utilization as reported in Fig. 8d. On the back of an electrochemical cell featuring WO_3 and Fe as the photoelectrode and reference electrode respectively, they integrated two polymeric layers: (i) the first layer, composed of a poly(octyl acrylate) matrix doped

with TTA-UC systems (PtOEP sensitizer and DPA emitter), upconverted green light into blue emission (~430 nm); (ii) the second layer, a poly (lauryl methacrylate) nanocomposite doped with CdSe/ZnS nanocrystals, absorbed yellow and green photons (unexploited by WO_3) and the TTA-UC layer, re-emitting strong green photoluminescence (at 522 nm with 30 nm bandwidth), which can be absorbed back by the upconverting layer and upconverted to blue light exploitable by the photocatalyst, creating a circular recycling photon scheme. This multilayer design boosted cell performance, leading to a 6.3% increase in photogenerated current compared to that of the same cell without these enhancements. Choi *et al.*[192] achieved photoelectrochemical water splitting by depositing a polymeric film containing TiO_2 nanoparticles coupled with a PdTPBP sensitizer-perylene annihilator TTA-UC system (capable of converting red light into blue) onto a 1% Mo-doped $BiVO_4$ photoanode. This configuration generated a photocurrent 17% higher compared to that of the photoanode without the upconversion film. Very recently Venkatesan *et al.*[193] developed a TTA-UC-enhanced PEC system by integrating a green-to-blue upconverting composite film with a 5% Mo-doped $BiVO_4$ photoanode. The upconverting film consisted of PtOEP sensitizer and DPA annihilator chromophores embedded in silica nanoparticles and mixed with a waterborne acrylic resin. This was coupled with Mo-doped $BiVO_4$ coated onto fluorine-doped tin oxide (FTO) glass. The PEC system simultaneously facilitated hydrogen evolution from water splitting at the photocathode and the photodegradation of enrofloxacin, a widely used fluoroquinolone antibiotic, at the photoanode. Under direct solar irradiation, nearly complete enrofloxacin degradation was achieved within 30 minutes under mild pH conditions, while the H_2 production rate reached 16.9 mmol g^{-1} h^{-1}, 1.5 times higher than that of the uncoated 5% Mo-doped $BiVO_4$ photoanode.[193]

4.1.2. Radical generation and photooxidation reactions. Radical generation is one of the main photocatalytic pathways, especially in environmental and biological reactions. Hydroxyl radicals were efficiently generated by combining TTA-UC materials encapsulated in a polymer shell with a platinum-loaded tungsten oxide (Pt/WO_3) photocatalyst. The system utilized the benchmark PtOEP/DPA upconversion green-to-blue UC sensitizer/acceptor pair.[194]

Another benchmark TTA-UC system (Pd based porphyrin/perylene as the sensitizer/acceptor) encapsulated in a silica shell and decorated with CdS QDs showed hydroxyl radical formation for coumarin degradation by upconverting red light to blue light.[195] A similar structure, adding a graphene oxide nanodisk as the cocatalyst was also applied to produce H_2O_2.[196] A double upconverting layered film strategy was applied to generate hydroxyl radicals for VOC oxidation.[197]

4.1.3. Organic reactions. In the synthesis of organic compounds, such as drugs, functional materials and fine chemicals, photoredox reactions promote radical generation and electron transfer. In this respect, for instance, inert aryl halides, such as C–Br and C–Cl, required UV light for their activation.[87]

One of the first photoredox reactions sensitized by TTA-UC was reported by Majek *et al.*,[182] involving the reductive activation of aryl–Br σ-bonds. The visible-to-UV photon upconversion system consisted of a metal-free dye (butane-2,3-dione) as the sensitizer and PPO as the triplet annihilator, enabling the activation of aryl bromides through a single-electron transfer (Scheme 4c).

Ravetz *et al.* demonstrated that IR light can drive various photoredox transformations through TTA-UC *via* different pathways (Scheme 4). Using Pt or Pd metal-center dyes as sensitizers along with TTBP or FDPP as the annihilator, they performed six different reactions, spanning from hydrodehalogenation to radical polymerization of methyl methacrylate (MMA) *via* C–Br bond reduction, upconverting IR light into orange and blue light.[179]

Another interesting study, performed by Liu *et al.*,[198] involves the use of a TTA-UC colloidal solution, composed of 5,10,15,20-tetra(*N*,*N*-diethylaniline)porphyrin palladium (PdTPNEt2P) as the sensitizer and perylene acting as the emitter and as the photocatalyst in a two-component configuration, to extract high-value products from a lignin-model compound ((2-(2-methoxyphenoxy)-1-(4-methoxyphenyl)ethanone)). The absorption of the incident radiation (λ_{exc} > 510 nm) from the sensitizer caused, through the TTA process, the excitation of perylene due to which, instead of emitting UC radiation, the singlet formed a radical anion through photoinduced electron transfer (Scheme 4c). This active species, then, converted a lignin model compound into two high-value products, namely 4-methoxyacetophenone and guaiacol, with a higher product selectivity, compared to the case in which just perylene was involved as the photocatalyst, working under higher-energy excitation radiation (λ_{exc} > 420 nm). This work highlights how using longer-wavelength light that can be converted by TTA-UC based photocatalysts, can reduce unwanted side reactions and provide a higher selectivity, compared to other traditional photocatalysts which do not take advantage of the TTA-UC process.

In 2020, Huang *et al.*[199] developed a high-performance TTA-UC photoredox system for the photooxidation of arylboronic acids to phenols. The system utilized a PdTPTNP sensitizer paired with six different perylene derivatives as annihilators. Notably, the combination with the lowest energy gap annihilator achieved the highest Φ_{UC}, reaching 8.35% under 653 nm laser irradiation and 7.05% under 720 nm LED light, with an upconverted emission peak at around 575 nm. By integrating this UC system with eosin Y as a photocatalyst and diacetoxyiodobenzene as an oxidizing agent in DMF solvent, the product yield increased to 78.2%, compared to 76% when using only the green-absorbing eosin Y photocatalyst. Beyond improved efficiency, TTA-UC-sensitized photocatalysts offer two key advantages: reduced photocatalyst photobleaching and minimized efficiency loss in large-scale reactions due to the deeper penetration of NIR light into colored systems. Specifically, when the reaction volume was increased from 2 to 20 mL, the product yield dropped significantly (from 76% to 28%, a ~63% decrease). In contrast, under NIR irradiation with TTA-UC, the decrease was much smaller (~23%), from 78.2% to 60%.[199]

Research on using QDs as sensitizers for TTA-UC in photocatalysis is still in its early stages, with significant progress needed to broaden the range of chemical reactions where these nanocomposites can act as effective photocatalysts. The main challenge lies in enhancing their Φ_{UC} to match the performance of molecular dye-sensitized TTA-UC systems.[37] A very interesting system was proposed by Liang *et al.*[14] They developed a colloidal TTA-UC system using a zinc-doped $CuInSe_2$ core or/and ZnS shell (ZCISe) as NIR absorbing photosensitizers (Fig. 5b). These QDs were capped with tetracene ligands to enable TET to rubrene, the annihilator, generating efficient NIR-to-yellow UC photons with an external quantum efficiency of 16.7%. This upconverted light was harnessed for multiple photochemical transformations (Fig. 9a). First, the system successfully facilitated the reductive dehalogenation of α-bromoacetophenone to acetophenone, achieving a product yield exceeding 99%. In this system, rubrene played a dual role as an annihilator and as a photocatalyst (system at two components). In control experiments, in its absence, or in absence of light or the TCA ligand, the product yield was negligible, confirming the need of the TTA-UC process to create the excited state of rubrene, responsible for the reaction. Furthermore, acetophenone could react with nucleophilic phenol, forming phenyl benzoate in a cascade reaction. In addition to reductive processes, the same TTA-UC system enabled the photo-oxidation of tetrahydrobenzothiazole to benzothiazole under 800 nm irradiation. Very recently Jiang *et al.*[61] demonstrated an efficient TTA-UC system for photocatalytic reactions driven by NIR-II (1000–1700 nm) light (Fig. 9b). They designed UC nanocomposites consisting of PbS QD sensitizers capped with Th-DPP mediators and coupled with rubrene annihilators. By converting NIR (1064 nm) photons into yellow ones, with a Φ_{UC} close to 0.19%, they induced the photopolymerization of a mixture composed of methyl methacrylate and ethylene glycol dimethacrylate monomers with ethyl α-bromophenylacetate as the photoinitiator within just five minutes (Fig. 9b). In contrast, the PbS/rubrene counterpart exhibited minimal polymerization under identical conditions, indicating that Th-DPP plays a crucial role in facilitating TET from PbS QDs to rubrene to drive the polymerization process. Additionally, in control experiments, no gel formation was observed when the reaction was conducted in air or without light, further confirming the important role of an efficient TTA-UC mechanism under NIR light.

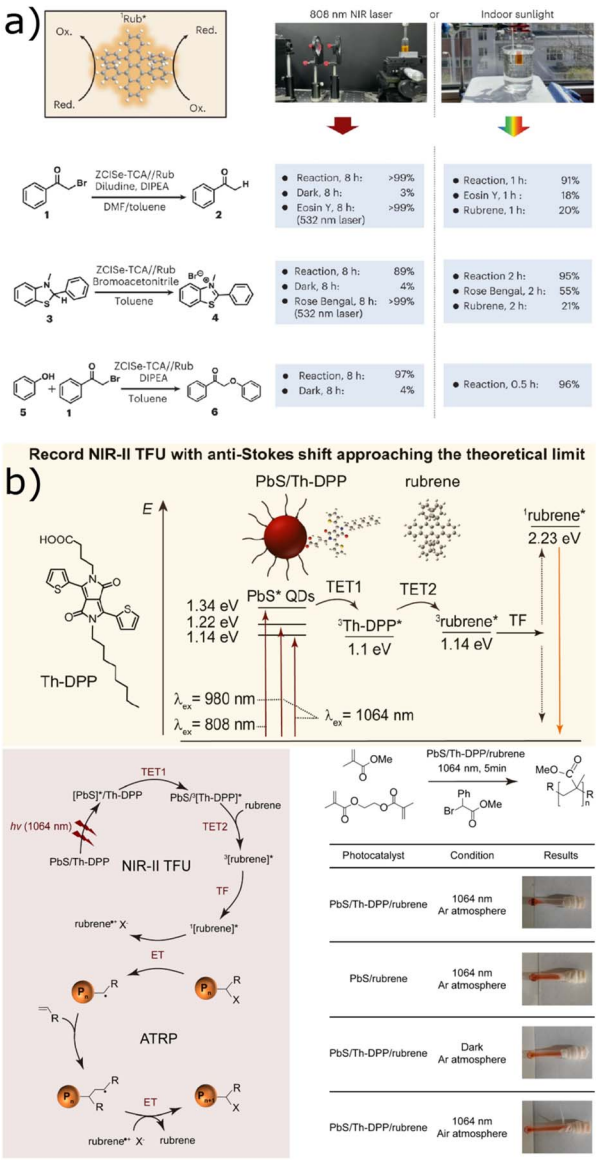

Fig. 9 (a) ZCISe QD sensitized TTA-UC using rubrene for photoredox organic synthesis and polymerization: the schematic, the picture of the system and the different reactions and parameters; reproduced from ref. 14 with permission from Springer Nature, Copyright 2023; (b) schematic illustration of PbS with a Th-DPP ligand and rubrene as the annihilator. The proposed mechanism and the recap of the different experimental conditions for polymerization are given below. Reproduced from ref. 61 with permission from American Chemical Society, Copyright 2024.

4.2. Other applications

4.2.1. Photovoltaics. Photovoltaics has been the first field explored to exploit TTA-UC systems.[176] Integrating the TTA-UC process into solar panels offers the potential to absorb and convert the NIR portion of the solar spectrum, addressing a key limitation of traditional silicon solar cells. Specifically, this could help to overcome the Shockley–Queisser limit, which sets the theoretical maximum efficiency of an ideal single p–n junction silicon solar cell with a 1.34 eV band-gap at approximately 33.16%, under standard solar conditions (AM 1.5 solar spectrum and 1 sun illumination). This efficiency cap arises from various energy loss mechanisms, including radiative electron–hole recombination, thermalization losses (*e.g.* heat dissipation from higher band-gap energy photons relaxing in the conduction band and electron–phonon inelastic interactions) and the inability of sub-band gap photons to be absorbed, leading them to be transmitted or reflected instead.[29,200,201] This last energy loss can be mitigated by extending the absorption range of the solar device through UC integration, potentially pushing the solar-to-electrical conversion limit up to ~48%.[37,202]

Several studies have explored the enhancement of solar cell performance by integrating the TTA-UC process. Initially, most

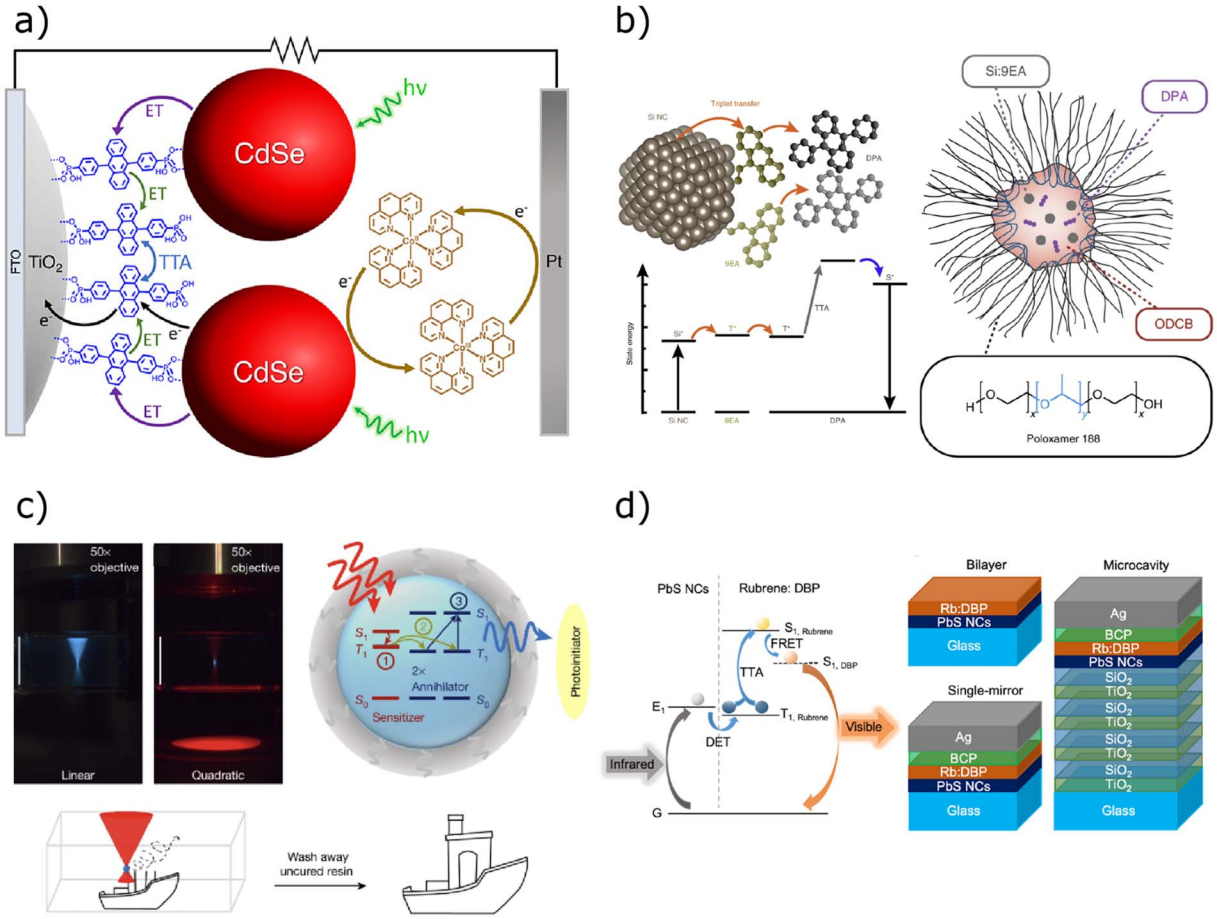

Fig. 10 (a) Schematic illustration of a TiO_2 photoanode coupled with a CdSe-sensitized TTA-UC system; reproduced from ref. 177 with permission from American Chemical Society, Copyright 2020; (b) cartoon of a Si QD sensitized TTA-UC system and the water soluble upconverting micelles; reproduced from ref. 48 with permission from Springer Nature, Copyright 2019; (c) photos illustrating the propagation of blue light through a medium with linear absorption and red light through a medium exhibiting quadratic absorption, with a focusing lens in place. Schematic of the upconversion process occurring for TTA-UC in 3D printing application and how the printing process is facilitated by using monovoxel excitation; reproduced from ref. 205 with permission from Springer Nature, Copyright 2022; (d) schematic of PbS QD sensitized TTA-UC with rubrene and the structure of the bilayer, single-mirror, and microcavity devices. Reproduced from ref. 206 with permission from American Chemical Society, Copyright 2021.

of these studies referred to UC nanocomposites in colloidal solutions. Over time, however, more practical solid-state systems have been developed.[202–204] Despite their convenience from an industrial point of view, solid state TTA-UC systems typically exhibit a lower Φ_{eff} compared to their colloidal counterparts. This reduction arises from factors such as limited emitter diffusion, which lowers the intermolecular collision rate and thus decreases the TTA probability as well as emitter aggregation in the planar structure, which reduces the fluorescence quantum yield. In the case of QD-sensitized TTA-UC, this results in a significant drop in Φ_{UC}, for example from 12% in a colloidal system to about 3.5% in the solid state configuration.[34,37,118]

Beery *et al.*[177] reported a solar device composed of fluorine-doped tin oxide (FTO) glass, coated by a TiO_2 film covered by a TTA-UC-based film (Fig. 10a). The UC layer consisted of CdSe QDs as the sensitizer, capped by oleic acid ligands and 4,4′-(anthracene-9,10-diyl) bis(4,1-phenylene) diphosphonic acid as the annihilator. The device, irradiated by a green light laser, was able to produce a short circuit current density (J_{SC}) of 29 μA cm^{-2} which however was much lower compared to that in a previous study, in which PtTCPP organometallic dye (Pt(II) tetrakis(4-carboxyphenyl)porphyrin) was employed as a sensitizer ($J_{SC} \approx 185$ μA cm^{-2}), under the same illumination conditions. This has been attributed to several causes, like an under unity energy transfer yield from QDs to the annihilator (40 to 80%), slow kinetics of regeneration and competitive QD excited state quenching induced by the electron mediator.[207]

4.2.2. Biological and medical applications. TTA-UC systems are very promising in biological and biomedical applications, including biosensing, bioimaging, and therapeutic treatments such as photocages.[87,175] TTA-mediated photo-uncaging can be applied both to detect tumors and to release cancer antigens, following either ET or eT pathways (Scheme 4).

Lanthanide-based compounds were largely applied in UC systems, for their sharp fluorescence profile with their larger anti-Stokes shift. However, TTA-UC systems are particularly

suited for biological uses thanks to their good efficiency under low-intensity excitation, since NIR light can penetrate tissues more effectively and with lower potential damage.[13,37,208] Yet, oxygen-induced quenching of triplet states can hinder the TTA-UC performance, especially in biological environments. To mitigate this, encapsulation with non-toxic organic materials (*i.e.*, fatty acids or paraffins) or inorganic coatings (such as SiO_2 shells) is often employed (see Section 4.3).[68]

For instance, Lee *et al.*[209] integrated a TTA-UC configuration into mesoporous silica microcapsules to enhance stability in aqueous systems and in the presence of oxygen. Their system, composed of PdTPBP as the sensitizer and perylene as the annihilator, upconverted red light ($\approx$640 nm) into blue emission (450 to 550 nm) with an Φ_{UC} = 3.40%. These nanocomposites were applied to tumor-targeted bioimaging. Following cytotoxicity testing, the silica-coated TTA-UC particles were incubated with tumor-tropic cells and irradiated with red light, producing visible blue-light emission (visible by the naked eye) and confirming effective cell binding through bright-field imaging.[209]

In photodynamic therapy, host/guest nanorod tetracene/pentacene as the TTA system, under 650 or 808 nm laser irradiation, efficiently generated singlet oxygen with a significantly higher quantum yield (74%) compared to a system without TTA (28%). *In vivo* studies demonstrated strong antitumor activity achieving cancer inhibition rates of 99% and 95% under 650 and 808 nm irradiation, respectively.[210]

The use of QD-sensitized TTA-UC systems in biomedical fields remains limited. Challenges include the relatively lower Φ_{UC} of QD-based systems compared to organic dye sensitizers and the cytotoxicity of common QDs containing Cd, Pb, or As. However, non/less-toxic NCs offer a very promising alternative as low-energy light absorbers. For instance Xia *et al.*[48] demonstrated the stability of Si-QD sensitizers capped with a 9EA mediator and paired DPA emitters under environmental conditions when encapsulated into non-toxic micelles (Fig. 10b). These green/red-to-blue upconverting nanocomposites maintained stability in aqueous, oxygen-rich environments, making them suitable for biological applications.[48] Recently, Peng *et al.*[211] developed TTA-UC nanoparticles by incorporating a TTA-UC pair, comprising a PtTPTNP sensitizer and a 9-ethynyl-10-phenylethynyl anthracene derivative annihilator acting as the photocatalyst as well (system at two components), into cinnamyl acetate nanodroplets. These nanodroplets were then encapsulated within an amphiphilic copolymer-based shell.

The resulting nanoparticles were tested as photocatalysts for a reversible reaction commonly occurring in biological systems. Their remarkable NIR-to-blue upconverted emission (with an impressive anti-Stokes shift of 0.76 eV) and an initial Φ_{UC} of 15.5%, which decreased to 1.8% after encapsulation, enabled efficient photoinduced cycling of the enzyme cofactor NADH to NAD^+ oxidation and NAD^+ to NADH reduction. This process, facilitated by glucose dehydrogenase as a reducing agent and glucose as an electron donor, was successfully sustained for over five cycles.[211]

4.2.3. Advanced manufacturing. Recently, TTA-UC has also found use in stereolithography technology thanks to its nonlinear optical features in a low power density range, enabling submicron resolution due to the confined excitation region. Additionally, the ability to operate under low-power and low-energy light reduces unwanted side reactions and damage to non-targeted areas, enhancing scalability for industrial applications.[68,212,213]

Limberg *et al.*[174] demonstrated submicron-resolution 3D printing using a TTA-UC system based on the energy transfer from the singlet to the photoinitiator. The system was formed by palladium(II)octaethylporphine (PdOEP) sensitizers and DPA emitters embedded in a photoresin. Green light excited the PdOEP sensitizers, initiating TET to DPA. After TTA, the resulting singlet-state energy of the emitter was directly transferred to the photoinitiator, triggering polymerization of the resin itself rather than radiative decay and photon emission.[174] Wong *et al.*[213] used a PdTPTBP/TIPS-anthracene TTA-UC system to cure polymer networks in opaque hydrogel composites with conventional radiation. In a hydrogel containing 1% TiO_2, red light (660 nm) activation of the TTA-UC system achieved a significantly higher cure rate (81.83%) and more uniform curing compared to UV light (365 nm), which resulted in a lower cure rate (64.7%) and incomplete polymerization.

Another interesting approach for 3D printing was the silica encapsulation of acid nanodroplet micelles containing upconversion materials, further decorated with covalently bound PEG based ligands (Fig. 10c). These components were then introduced into a resin formed by using commercially available materials.[205]

4.3. TTA-UC encapsulation

A major challenge for efficient UC in photocatalysis and all the other oxygen-exposed applications is preventing the quenching of upconverted emission. In both liquid and solid-state TTA-UC systems, the presence of molecular oxygen significantly limits versatility, scalability, and practical implementation in light-driven technologies. A molecule of oxygen possesses a triplet-ground state/singlet-excited state energy gap of around 0.98 eV, which potentially enables the energy transfer from sensitizer/annihilator triplets to the spin-allowed triplet ground state of O_2.[67] When the gap between T_{1s}/S_{0s} and T_{1a}/S_{0a} is higher than this threshold value, the number of upconverted photons is drastically decreased (with a decrease in PLQY going from 10% to over 90%).[72] This can happen because of T_{1s} and T_{1a} electrons decaying to the oxygen triplet-ground state or S_{1a} electrons decaying back to T_{1s} by transferring energy to the oxygen triplet-ground state.[214] Either the triplet state of the sensitizer or the annihilator can efficiently sensitize oxygen molecules, generating singlet oxygen.[215] Conversely in some systems where the T_{1s}/S_{0s} and T_{1a}/S_{0a} energy gap is lower than 0.98 eV, the presence of oxygen seems to even cause an increase in Φ_{eff}, as reported by Gholizadeh *et al.*[70] Wang *et al.*[72] recently proposed an oxygen-resistant near-infrared TTA-UC system based on non-organometallic cyanine sensitizers (λ_{ex} = 808 nm) and specially designed quinoxaline-based dye dimers as annihilators (λ_{em} =

650 nm), having LUMO energy levels of around −3.7 eV, a threshold known to enhance the long-term stability of organic molecules.[72]

For TTA-UC systems whose exposure to molecular oxygen can be detrimental, the general trend consists of encapsulating both sensitizer and annihilator moieties based on the sensitizer/emitter system properties, and on the solvent/matrix affinity.[67]

Typically the main strategies as oxygen barriers for TTA-UC systems include (Fig. 11a): (i) lipid nanoemulsions/nanodroplets, (ii) liposomes, (iii) polymer-based nanoparticles, (iv) silica-coated nanoparticles, and (v) metal–organic frameworks (MOFs).[67,68] Liposome encapsulation has been shown to be a particularly efficient technique, since it not only minimizes upconverted emission losses caused by oxygen-induced quenching but also enhances the solubility of TTA-UC systems in polar media, an essential feature for biological applications. Additionally, embedding both the sensitizer and annihilator within the liposome nanostructure increases their local concentration, thereby improving the probability of TET. For instance, Brion *et al.*[217] incorporated a TTA-UC system, consisting of a PdTPTBP sensitizer and a *tert*-butylated perylene emitter, into photoactivable liposomes functionalized with the anti-tumor drug melphalan. Upon red-light absorption, the upconversion nanoparticles emitted light with two distinct maxima in the green and blue spectral regions, triggering the photocleavage of the linker with an 86% release of the total drug payload, effectively inducing tumor cell death *in vitro*.[217] Polymer-based encapsulation offers promising potential as well. Self-assembling block copolymers in micelles can functionalize encapsulating layers, enabling solubility in various media.[67,218,219]

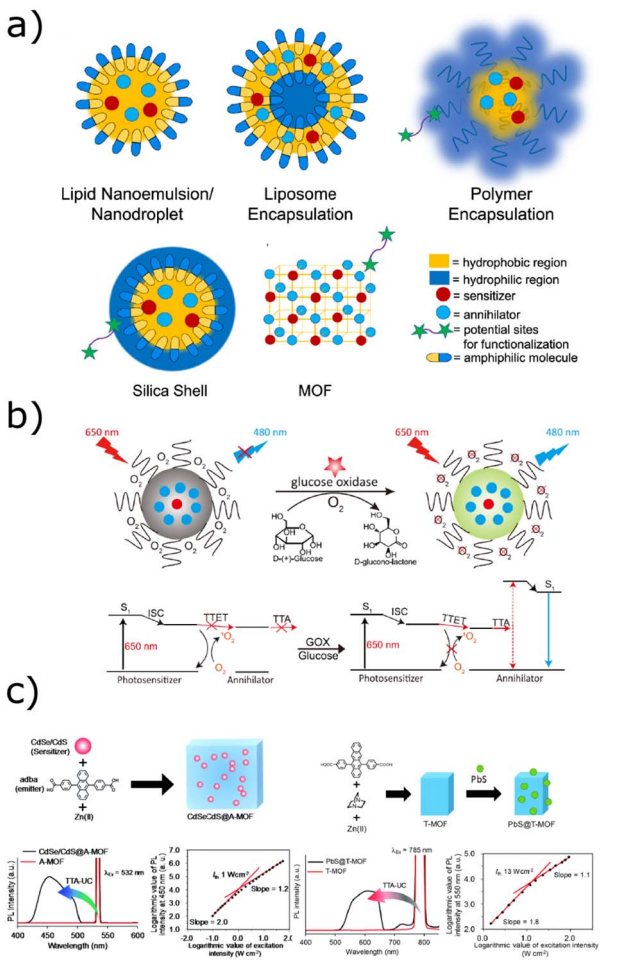

Fig. 11 (a) Scheme reporting the main encapsulation methods for TTA-UC systems, to avoid oxygen-induced quenching of the upconverted emission. Reproduced with permission from ref. 67 Copyright 2023 American Chemical Society; (b) schematic illustration and mechanism of activating TTA-UC nanoparticles in the presence of glucose and glucose oxidase (GOX) to address the oxygen-quenching issue. Reproduced from ref. 215 with permission from Springer Nature, Copyright 2021; (c) cartoon of CdSe/CdS@A-MOF for green to blue light UC and PbS@T-MOF for NIR to visible light UC; the upconverted emission spectra and the graphs show the PL *vs.* I_{th}; reproduced from ref. 216 with permission from Royal Society of Chemistry, Copyright 2018.

Silica shell encapsulation, as mentioned previously, effectively protects TTA-UC systems from oxygen quenching and moisture, reducing TTA losses while preventing component aggregation.[68] Its stability, hardness, and biocompatibility make it ideal for solar energy conversion and bioimaging.[68,71] Lee *et al.*[220] encapsulated TTA-UC systems in hollow mesoporous silica nanoparticles for thermal energy storage and smart drug delivery applications, by incorporating PdTPBP sensitizers, perylene annihilators, and 2,4-hexadien-1-ol as additional oxygen protection. MOFs,[221] a class of two-or three-dimensional porous crystalline materials with exceptionally high surface areas, have recently been explored as platforms for TTA-UC systems, where the choice of MOF ligand, porosity, and optical properties can be tailored to enhance stability, prevent oxygen quenching, and facilitate electronic transitions and charge transfer for efficient TTA-UC.[67] Compared to other TTA-UC encapsulations, MOFs offer distinct advantages, particularly in their precise control over solubility and structural organization. Furthermore, the ability to fine-tune the ratio of sensitizers and annihilators within the MOF matrix allows for improved energy transfer efficiency by adjusting the spatial arrangement and orientation of the embedded chromophores. Some studies suggest that the hydrophobic microenvironments within certain MOFs may help mitigate oxygen quenching, enhancing their potential for TTA-UC applications.[67,222] Furthermore, MOF frameworks have also been utilized to develop nanocrystal-based TTA hybrids, which have emerged as a promising strategy for solid-state upconverters, as discussed in Section 4.3.2. The progress made so far in encapsulating TTA systems is promising, showing potential for long-term stability and protection against oxygen-induced exciton quenching. It also enhances solubility and functionalization, making TTA-UC systems suitable for a broader range of applications. However, further work is needed to address the significant decrease in Φ_{eff} after encapsulation, which is primarily linked to the aggregation of UC moieties when confined within the protective shell.

4.3.1. TTA-UC in aqueous solution. An interesting strategy to apply the TTA-UC process in water solution was the enzymatic application of the glucose oxidase (GOX)-catalyzed

glucose oxidation reaction which can efficiently remove oxygen (Fig. 11b).[215] A PdTPBP and perylene dye pair (sensitizer/annihilator) was encapsulated in an amphiphilic polymer and used in the presence of the GOX enzyme to control the oxygen level. By monitoring the upconversion emission, the authors also showed that this strategy can be used to create TTA-based biosensors.[215] Very recently, six amino acids were identified as oxygen scavengers for use in TTA-UC-based sensing to detect herbicide residues, specifically paraquat, a common but highly toxic water-soluble herbicide.[223] This study demonstrates the potential of TTA-based sensors for real-world applications. In this system, the negatively charged carboxylic acid groups on the surface of TTA-UC nanoparticles (using a PdTPBP and perylene dye pair for red-to-blue upconversion) facilitate the electrostatic adsorption of the positively charged paraquat. Upon exposure to red light, photoinduced electron transfer from the triplet-excited photosensitizer to the adsorbed paraquat forms a paraquat radical anion, quenching the triplet state of PdTPBP. This reduces the triplet energy transfer to perylene, leading to a decrease in upconversion luminescence intensity, which can be correlated with the concentration of the herbicide. Among the amino acids studied, methionine and histidine showed the fastest singlet oxygen trapping characteristics, thereby promoting a quick recovery of the TTA-UC luminescence.

4.3.2. TTA-UC in solid state applications. Solid-state systems, consisting of TTA-UC nanoparticles embedded in a solid-state matrix, have also been explored, especially for solar devices, but also for bio-applications or electronic devices (*e.g.* LEDs).[224,225] Although their Φ_{eff} is typically lower than that of solution-based UCS (mainly because of the reduced nanoparticle mobility, which limits triplet diffusion and annihilation), these solid-state systems offer greater environmental stability and practicality. They are better suited for real-world applications, as they can be more easily integrated into other devices.[127]

For example, in one of the first applications, Miteva *et al.*[226] successfully created a flexible display based on TTA-UC by embedding UC nanoparticles into a transparent styrene oligomer matrix. The nanoparticles comprised combinations of PdTPBP as sensitizers paired with different annihilators: rubrene (λ_{em} = 560 nm), BPEA (λ_{em} = 513 nm), and perylene (λ_{em} = 475 nm). The system was effectively excited by low-power 633 nm radiation, demonstrating the feasibility of flexible TTA-UC-based displays.

In the last decade, several studies have pushed the integration of UC layers into solar cells. A key milestone was achieved by Wu *et al.* who pioneered the use of PbS QDs as sensitizers in solid-state UC devices (Fig. 3b). These nanocrystals were coupled with rubrene as the annihilator phase, and doped with DBP, upconverting light from $\lambda > 1$ μm to visible through an efficient Dexter ET (Scheme 4).[112] In subsequent studies, researchers investigated the relationship between PbS thickness and upconverted light intensity, identifying two major challenges that significantly reduced UC efficiency:[34,227] (i) the rapid back-transfer of singlet excitons, generated through TTA, to PbS nanocrystals *via* FRET, and (ii) inefficient energy transfer between Pb QDs, which hinders exciton transfer to rubrene beyond a monolayer.[5] To address some of these issues, Wu *et al.*[206] integrated PbS-rubrene upconverting layers into a Fabry–Pérot microcavity, which enhanced IR light absorption and increased UC emission by over two orders of magnitude, in the presence of a back mirror and an optical space layer (Fig. 10d). However, despite these refinements, external quantum efficiency remained below 1% due to persistent losses from inefficient exciton transfer.[206]

To obtain TTA-UC solid state devices, a range of innovative approaches is being explored. For instance, nanocrystal–MOF hybrids have emerged as a promising strategy for solid-state TTA-UC, demonstrated by the combination of visible CdSe/CdS QDs with an anthracene-based MOF for green-to-blue upconversion and NIR PbS QDs with a tetracene-based MOF for NIR-to-visible upconversion (Fig. 11c).[216] These hybrid materials enhance energy transfer efficiency and open new avenues for expanding TTA-UC applications in solid-state systems. Two distinct methods for integrating nanocrystals with MOFs were explored: (i) incorporating nanocrystals during MOF crystallization and (ii) post-synthetically modifying the MOF surface with nanocrystals. While the Φ_{UC} remained low (with a maximum reported value of 0.0009%), likely due to inefficient energy transfer between the nanocrystals and the MOF-embedded annihilators, further optimization could enhance performance. Future advancements may involve rational modifications to MOF structures, integration with covalent organic frameworks (COFs), and the development of next-generation triplet sensitizers and annihilators with controlled spatial arrangement to optimize energy transfer efficiency. These improvements could lead to highly efficient solid-state upconverters capable of operating at low excitation intensities.

Another approach was pursued by Rigsby *et al.*,[119] who embedded TTA-UC nanoparticles composed of CdSe NCs coupled with DPA emitters into a wide-bandgap polymeric (poly(9-vinylcarbazole)) matrix. This resulted in a thin film able to upconvert green light (λ_{exc} = 532 nm) into blue light, with the most intense emission peak centered at around 450 nm and $\Phi_{UC} \approx 1.5\%$.

5. Conclusions and future perspectives

The research related to TTA-UC systems is still in its earlier stages and more efforts are required to enhance their performances. Specifically NCs have emerged as a promising class of sensitizer materials for photon upconversion, yet their performance still falls short compared to their molecular dye-based counterparts. The ability to precisely control the optoelectronic properties of semiconductor NCs through fine-tuning their size, shape, composition, and defect states, offers a clear path toward improving their upconversion efficiency. Core–shell engineering and optimized ligand mediator design can enhance triplet energy transfer while ensuring high Φ_{eff}, even under ambient conditions where oxygen quenching is a challenge. Additionally, strategic band alignment remains a crucial factor in maximizing the efficiency of upconverted photon generation.

The development of non/less-toxic NCs, particularly ternary I–III–VI QDs, holds significant promise for overcoming existing limitations. These materials exhibit broad and intense absorption spectra, strong defect tolerance, and unique excitonic properties such as exciton "self-trapping," which enables prolonged exciton lifetimes. Such features have already led to some of the highest Φ_{eff} values reported for NC-sensitized TTA-UC systems. Expanding the selection of annihilators and further optimizing the upconversion process could unlock applications in solar energy harvesting and other optoelectronic fields.

Beyond solar energy, the nonlinear optical properties of the TTA-UC process open new routes for bioimaging, biomedicine, precise 3D printing and photo-driven chemical reactions. The ability to achieve upconversion beyond the bandgap of crystalline silicon, with excitation wavelengths in the NIR, highlights the versatility of NC-based TTA-UC systems. In photo-driven reactions, especially in solar fuel production (*e.g.* H_2 production and CO_2 conversion), TTA-UC systems can enhance the utilization of available photons from total solar irradiation, enabling more efficient driving of these challenging chemical reactions. However, to fully leverage their potential, several challenges must be addressed. These include mitigating exciton/electron pathway losses, developing synthesis techniques for highly uniform and stable NCs, and improving long-term photostability under continuous irradiation. Novel strategies such as heterostructure designs and encapsulation can play a pivotal role in addressing these issues and achieving scalable technologies. Recent advancements in encapsulation techniques (Section 4.3), including the use of mesoporous silica shells, polymeric matrices, nanodroplets, MOF integration, and coupling with enzymes have shown promise in protecting TTA-UC systems from oxygen quenching, enhancing solubility, and maintaining structural integrity. Additionally, multi-layered architectures and hybrid materials have been explored to amplify light absorption and improve energy transfer efficiency (Section 3). Furthermore, machine learning approaches and automated screening platforms[228] are expected to accelerate the discovery and optimization of novel strategies in designing NC sensitized-TTA-UC systems with enhanced performance, stability, and scalability.

In conclusion, NC-based TTA-UC represents a transformative approach to photon management, with applications spanning from sustainable energy to biomedicine. While significant progress has been made, continued research is essential to refine material design, improve system stability, and enhance overall efficiency. The interdisciplinary nature of this field promises exciting breakthroughs, paving the way for next-generation light-harvesting and optoelectronic systems that push the boundaries of current technology. Through this review, we hope to spark curiosity to inspire further research in this area, paving the way for substantial improvements in the performance and stability of these systems to ensure their application in the real world.

Data availability

This review does not include original research data, software, or code, and no new experimental data were generated.

Author contributions

MB: writing the original draft; FSF: conceptualization, methodology, writing review and editing, resources, supervision; BB: conceptualization, editing, supervision, financial support.

Conflicts of interest

The authors declare no conflicts of interest.

Acknowledgements

This study was carried out within the «GREEN UP: GREENER NANOMATERIALS FOR UPCONVERSION IN PHOTOCATALYTIC APPLICATIONS» project – funded by the Ministero dell'Università e della Ricerca – within the PRIN 2022 program (D.D.104-02/02/2022) funded by the European Union – Next Generation EU. This manuscript reflects only the authors' views and opinions, and the Ministry cannot be considered responsible for them. MB thanks support from the MUR for the PhD project "Synthesis and characterization of photocatalysts enhanced by upconversion systems and/or plasmonic nanomaterials to exploit sunlight in reactions of environmental interest" (DM 118/PNRR).

References

1 C. A. Parker and C. G. Hatchard, *Proc. R. Soc. London, Ser. A*, 1962, **269**, 574–584.
2 J. Chen and J. X. Zhao, *Sensors*, 2012, **12**, 2414–2435.
3 R. T. Wegh, H. Donker, E. V. D. Van Loef, K. D. Oskam and A. Meijerink, *J. Lumin.*, 2000, **87–89**, 1017–1019.
4 Y. Zhang, W. Du and X. Liu, *Nanoscale*, 2024, **16**, 2747–2764.
5 J. Alves, J. Feng, L. Nienhaus and T. W. Schmidt, *J. Mater. Chem. C*, 2022, **10**, 7783–7798.
6 N. Yanai and N. Kimizuka, *Acc. Chem. Res.*, 2017, **50**, 2487–2495.
7 R. R. Islangulov, D. V. Kozlov and F. N. Castellano, *Chem. Commun.*, 2005, 3776–3778.
8 J. C. Johnson, A. J. Nozik and J. Michl, *Acc. Chem. Res.*, 2013, **46**, 1290–1299.
9 A. Rao and R. H. Friend, *Nat. Rev. Mater.*, 2017, **211**(2), 1–12.
10 Q. Liu, W. Feng, T. Yang, T. Yi and F. Li, *Nat. Protoc.*, 2013, **810**, 2033–2044.
11 Y. Ma, J. Bao, Y. Zhang, Z. Li, X. Zhou, C. Wan, L. Huang, Y. Zhao, G. Han and T. Xue, *Cell*, 2019, **177**, 243–255.
12 Y. Hu, B. Xu, W. Li, L. Liang, F. Fei and Q. Lin, *J. Nanobiotechnol.*, 2024, **22**, 1–10.
13 J. Zhou, Q. Liu, W. Feng, Y. Sun and F. Li, *Chem. Rev.*, 2015, **115**, 395–465.
14 W. Liang, C. Nie, J. Du, Y. Han, G. Zhao, F. Yang, G. Liang and K. Wu, *Nat. Photonics*, 2023, **17**, 346–353.
15 P. Bharmoria, H. Bildirir and K. Moth-Poulsen, *Chem. Soc. Rev.*, 2020, **49**, 6529–6554.
16 B. Joarder, N. Yanai and N. Kimizuka, *J. Phys. Chem. Lett.*, 2018, **9**, 4613–4624.

17 V. Gray, K. Moth-Poulsen, B. Albinsson and M. Abrahamsson, *Coord. Chem. Rev.*, 2018, **362**, 54–71.
18 R. R. Islangulov, J. Lott, C. Weder and F. N. Castellano, *J. Am. Chem. Soc.*, 2007, **129**, 12652–12653.
19 R. R. Islangulov and F. N. Castellano, *Angew. Chem., Int. Ed.*, 2006, **45**, 5957–5959.
20 T. N. Singh-Rachford and F. N. Castellano, *Inorg. Chem.*, 2009, **48**, 2541–2548.
21 S. Baluschev, J. Jacob, Y. S. Avlasevich, P. E. Keivanidis, T. Miteva, A. Yasuda, G. Nelles, A. C. Grimsdale, K. Müllen and G. Wegner, *ChemPhysChem*, 2005, **6**, 1250–1253.
22 S. Baluschev, T. Miteva, V. Yakutkin, G. Nelles, A. Yasuda and G. Wegner, *Phys. Rev. Lett.*, 2006, **97**, 143903.
23 Y. Niihori, T. Kosaka and Y. Negishi, *Mater. Horiz.*, 2024, **11**, 2304–2322.
24 K. Börjesson, P. Rudquist, V. Gray and K. Moth-Poulsen, *Nat. Commun.*, 2016, **7**, 12689.
25 Y. Han, S. He and K. Wu, *ACS Energy Lett.*, 2021, **6**, 3151–3166.
26 N. Kimizuka, N. Yanai and M. A. Morikawa, *Langmuir*, 2016, **32**, 12304–12322.
27 Y. Zhou, F. N. Castellano, T. W. Schmidt and K. Hanson, *ACS Energy Lett.*, 2020, **5**, 2322–2326.
28 N. Nishimura, V. Gray, J. R. Allardice, Z. Zhang, A. Pershin, D. Beljonne and A. Rao, *ACS Mater. Lett.*, 2019, **1**, 660–664.
29 L. Naimovičius, P. Bharmoria and K. Moth-Poulsen, *Mater. Chem. Front.*, 2023, **7**, 2297–2315.
30 M. Uji, T. J. B. Zähringer, C. Kerzig and N. Yanai, *Angew. Chem., Int. Ed.*, 2023, **62**, e202301506.
31 S. Xu, Y. Yuan, X. Cai, C.-J. Zhang, F. Hu, J. Liang, G. Zhang, D. Zhang and B. Liu, *Chem. Sci.*, 2015, **6**, 5824–5830.
32 Z. Jiang, Y. Liu, Y. Yang, T. Guan, C. Qin and Y. Liu, *Opt. Lett.*, 2024, **49**, 6940.
33 Z. Huang, Z. Xu, T. Huang, V. Gray, K. Moth-Poulsen, T. Lian and M. L. Tang, *J. Am. Chem. Soc.*, 2020, **142**, 17581–17588.
34 L. Nienhaus, M. Wu, N. Geva, J. J. Shepherd, M. W. B. Wilson, V. Bulović, T. Van Voorhis, M. A. Baldo and M. G. Bawendi, *ACS Nano*, 2017, **11**, 7848–7857.
35 S. K. Sugunan, U. Tripathy, S. M. K. Brunet, M. F. Paige and R. P. Steer, *J. Phys. Chem. A*, 2009, **113**, 8548–8556.
36 S. Baluschev, V. Yakutkin, G. Wegner, B. Minch, T. Miteva, G. Nelles and A. Yasuda, *J. Appl. Phys.*, 2007, **101**, 5–8.
37 Z. Huang, C. H. Tung and L. Z. Wu, *Acc. Mater. Res.*, 2024, **5**, 136–145.
38 L. Hou, A. Olesund, S. Thurakkal, X. Zhang and B. Albinsson, *Adv. Funct. Mater.*, 2021, **31**, 2106198.
39 S. He, X. Luo, X. Liu, Y. Li and K. Wu, *J. Phys. Chem. Lett.*, 2019, **10**, 5036–5040.
40 R. Sun, J. Zang, R. Lai, W. Yang and B. Ji, *J. Am. Chem. Soc.*, 2024, **146**, 17618–17623.
41 Z. Xu, Z. Huang, C. Li, T. Huang, F. A. Evangelista, M. L. Tang and T. Lian, *ACS Appl. Mater. Interfaces*, 2020, **12**, 36558–36567.
42 P. Xia, Z. Huang, X. Li, J. J. Romero, V. I. Vullev, G. S. H. Pau and M. L. Tang, *Chem. Commun.*, 2017, **53**, 1241–1244.
43 Z. A. Vanorman, C. R. Conti, G. F. Strouse and L. Nienhaus, *Chem. Mater.*, 2021, **33**, 452–458.
44 K. Wang, R. P. Cline, J. Schwan, J. M. Strain, S. T. Roberts, L. Mangolini, J. D. Eaves and M. L. Tang, *Nat. Chem.*, 2023, **15**(8), 1172–1178.
45 Z. Huang, P. Xia, N. Megerdich, D. A. Fishman, V. I. Vullev and M. L. Tang, *ACS Photonics*, 2018, **5**, 3089–3096.
46 R. Lai, Y. Sang, Y. Zhao and K. Wu, *J. Am. Chem. Soc.*, 2020, **142**, 19825–19829.
47 P. Jaimes, T. Miyashita, T. Qiao, K. Wang and M. L. Tang, *J. Phys. Chem. C*, 2023, **127**, 1752–1757.
48 P. Xia, E. K. Raulerson, D. Coleman, C. S. Gerke, L. Mangolini, M. L. Tang and S. T. Roberts, *Nat. Chem.*, 2020, **12**, 137–144.
49 S. He, R. Lai, Q. Jiang, Y. Han, X. Luo, Y. Tian, X. Liu and K. Wu, *Angew. Chem., Int. Ed.*, 2020, **59**, 17726–17731.
50 Z. Huang, Z. Xu, M. Mahboub, X. Li, J. W. Taylor, W. H. Harman, T. Lian and M. L. Tang, *Angew. Chem. Int. Ed.*, 2017, **56**, 16583–16587.
51 Y. Han, S. He, X. Luo, Y. Li, Z. Chen, W. Kang, X. Wang and K. Wu, *J. Am. Chem. Soc.*, 2019, **141**, 13033–13037.
52 E. M. Rigsby, T. Miyashita, P. Jaimes, D. A. Fishman and M. L. Tang, *J. Chem. Phys.*, 2020, **153**, 114702.
53 X. W. Chua, L. Dai, M. Anaya, H. Salway, E. Ruggeri, P. Bi, Z. Yang, S. D. Stranks and L. Yang, *ACS Nano*, 2024, **18**, 15229–15238.
54 N. Gong, R. Lai, S. Xing, Z. Z. Liu, J. Mo, T. Man, Z. Li, D. Di, J. Du, D. Tan, X. Liu, J. Qiu and B. Xu, *Adv. Sci.*, 2023, **10**, 1–10.
55 S. He, Y. Han, J. Guo and K. Wu, *J. Phys. Chem. Lett.*, 2022, **13**, 1713–1718.
56 J. De Roo, Z. Huang, N. J. Schuster, L. S. Hamachi, D. N. Congreve, Z. Xu, P. Xia, D. A. Fishman, T. Lian, J. S. Owen and M. L. Tang, *Chem. Mater.*, 2020, **32**, 1461–1466.
57 X. Lin, Z. Chen, Y. Han, C. Nie, P. Xia, S. He, J. Li and K. Wu, *ACS Energy Lett.*, 2022, **7**, 914–919.
58 V. Gray, P. Xia, Z. Huang, E. Moses, A. Fast, D. A. Fishman, V. I. Vullev, M. Abrahamsson, K. Moth-Poulsen and M. Lee Tang, *Chem. Sci.*, 2017, **8**, 5488–5496.
59 X. Luo, G. Liang, Y. Han, Y. Li, T. Ding, S. He, X. Liu and K. Wu, *J. Am. Chem. Soc.*, 2020, **142**, 11270–11278.
60 R. Lai and K. Wu, *J. Chem. Phys.*, 2020, **153**, 114701.
61 L. H. Jiang, X. Miao, M. Y. Zhang, J. Y. Li, L. Zeng, W. Hu, L. Huang and D. W. Pang, *J. Am. Chem. Soc.*, 2024, **146**, 10785–10797.
62 Z. Huang, D. E. Simpson, M. Mahboub, X. Li and M. L. Tang, *Chem. Sci.*, 2016, **7**, 4101–4104.
63 A. Sahu and D. Kumar, *J. Alloys Compd.*, 2022, **924**, 166508.
64 Y. Y. Cheng, T. Khoury, R. G. C. R. Clady, M. J. Y. Tayebjee, N. J. Ekins-Daukes, M. J. Crossley and T. W. Schmidt, *Phys. Chem. Chem. Phys.*, 2010, **12**, 66–71.
65 A. R. Collins, B. Zhang, M. J. Bennison and R. C. Evans, *J. Mater. Chem. C*, 2024, **12**, 6310–6318.
66 A. Monguzzi, M. Frigoli, C. Larpent, R. Tubino and F. Meinardi, *Adv. Funct. Mater.*, 2012, **22**, 139–143.

67 T. Schloemer, P. Narayanan, Q. Zhou, E. Belliveau, M. Seitz and D. N. Congreve, *ACS Nano*, 2023, **17**, 3259–3288.
68 P. Venkatesan, P. Pal, S. S. Ng, J.-Y. Lin and R.-A. Doong, *Coord. Chem. Rev.*, 2025, **523**, 216266.
69 T. Ogawa, N. Yanai, A. Monguzzi and N. Kimizuka, *Sci. Rep.*, 2015, **5**, 10882.
70 E. M. Gholizadeh, S. K. K. Prasad, Z. L. Teh, T. Ishwara, S. Norman, A. J. Petty, J. H. Cole, S. Cheong, R. D. Tilley, J. E. Anthony, S. Huang and T. W. Schmidt, *Nat. Photonics*, 2020, **14**, 585–590.
71 W. Ahmad, J. Wang, H. Li, Q. Ouyang, W. Wu and Q. Chen, *Coord. Chem. Rev.*, 2021, **439**, 213944.
72 X. Wang, F. Ding, T. Jia, F. Li, X. Ding, R. Deng, K. Lin, Y. Yang, W. Wu, D. Xia and G. Chen, *Nat. Commun.*, 2024, **15**, 1–12.
73 T. W. Schmidt and F. N. Castellano, *J. Phys. Chem. Lett.*, 2014, **5**, 4062–4072.
74 N. Nishimura, J. R. Allardice, J. Xiao, Q. Gu, V. Gray and A. Rao, *Chem. Sci.*, 2019, **10**, 4750–4760.
75 K. Chen, Q. Luan, T. Liu, B. Albinsson and L. Hou, *Responsive Mater.*, 2024, e20240030.
76 M. Savastano, M. Passaponti, W. Giurlani, L. Lari, N. Calisi, E. Delgado-Pinar, E. S. Serrano, E. Garcia-España, M. Innocenti, V. K. Lazarov and A. Bianchi, *Angew. Chem.*, 2021, **518**, 120250.
77 S. Hisamitsu, N. Yanai and N. Kimizuka, *Angew. Chem., Int. Ed.*, 2015, **54**, 11550–11554.
78 A. Monguzzi, J. Mézyk, F. Scotognella, R. Tubino and F. Meinardi, *Phys. Rev. B:Condens. Matter Mater. Phys.*, 2008, **78**, 195112.
79 T. N. Singh-Rachford and F. N. Castellano, *J. Phys. Chem. Lett.*, 2010, **1**, 195–200.
80 H. C. Chen, C. Y. Hung, K. H. Wang, H. L. Chen, W. S. Fann, F. C. Chien, P. Chen, T. J. Chow, C. P. Hsu and S. S. Sun, *Chem. Commun.*, 2009, 4064–4066.
81 S. Guo, W. Wu, H. Guo and J. Zhao, *J. Org. Chem.*, 2012, **77**, 3933–3943.
82 J. Zhao, S. Ji and H. Guo, *RSC Adv.*, 2011, **1**, 937–950.
83 A. Ronchi and A. Monguzzi, *Chem. Phys. Rev.*, 2022, **3**, 041301.
84 L. Zeng, L. Huang, J. Han and G. Han, *Acc. Chem. Res.*, 2022, **55**, 2604–2615.
85 W. Lin, Z. Huang, L. Huang and G. Han, *Chem. Phys. Rev.*, 2024, **5**, 021301.
86 J. Jin, T. Yu, J. Chen, R. Hu, G. Yang, Y. Zeng and Y. Li, *Curr. Opin. Green Sustainable Chem.*, 2023, **43**, 100841.
87 L. Huang and G. Han, *Nat. Rev. Chem*, 2024, **8**, 238–255.
88 S. C. Zhu and F. X. Xiao, *ACS Catal.*, 2023, **13**, 7269–7309.
89 S. Baluschev, V. Yakutkin, T. Miteva, G. Wegner, T. Roberts, G. Nelles, A. Yasuda, S. Chernov, S. Aleshchenkov and A. Cheprakov, *New J. Phys.*, 2008, **10**, 013007.
90 K. Suzuki, A. Kobayashi, S. Kaneko, K. Takehira, T. Yoshihara, H. Ishida, Y. Shiina, S. Oishi and S. Tobita, *Phys. Chem. Chem. Phys.*, 2009, **11**, 9850–9860.
91 L. Prodi and M. T. Gandolfi, *Handbook of Photochemistry*, 2007, vol. 44.
92 F. Qi, H. J. Feng, Y. Peng, L. H. Jiang, L. Zeng and L. Huang, *ACS Appl. Mater. Interfaces*, 2024, **16**, 7512–7521.
93 C. M. Sullivan and L. Nienhaus, *Nanoscale*, 2022, **14**, 17254–17261.
94 C. M. Sullivan and L. Nienhaus, *Chem. Mater.*, 2024, **36**, 417–424.
95 A. L. Efros and L. E. Brus, *ACS Nano*, 2021, **15**, 6192–6210.
96 L. Brus, *Electronic Wave Functions In Semiconductor Clusters: Experiment and Theory*, 1986, vol. 90.
97 M. R. Kim and D. Ma, *J. Phys. Chem. Lett.*, 2015, **6**, 85–99.
98 F. S. Freyria, J. M. Cordero, J. R. Caram, S. Doria, A. Dodin, Y. Chen, A. P. Willard and M. G. Bawendi, *Nano Lett.*, 2017, **17**, 7665–7674.
99 Y. Chen, J. M. Cordero, H. Wang, D. Franke, O. B. Achorn, F. S. Freyria, I. Coropceanu, H. Wei, O. Chen, D. J. Mooney and M. G. Bawendi, *Angew. Chem., Int. Ed.*, 2018, **57**, 4652–4656.
100 G. Azzellino, F. S. Freyria, M. Nasilowski, M. G. Bawendi and V. Bulović, *Adv. Mater. Technol.*, 2019, **4**, 1–6.
101 H. Wu, X. Li, C. Tung and L. Wu, *Adv. Mater.*, 2019, **31**, 1900709.
102 H. Su, W. Wang, R. Shi, H. Tang, L. Sun, L. Wang, Q. Liu and T. Zhang, *Carbon Energy*, 2023, **5**, e280.
103 M. Yuan, X. Yan, J. N. Yuan, P. Su, Q. Chen and F. X. Xiao, *J. Catal.*, 2024, **437**, 115667.
104 P. Su, S. Li and F. X. Xiao, *Small*, 2024, **20**, 2400958.
105 K. Agarwal, H. Rai and S. Mondal, *Mater. Res. Express*, 2023, **10**, 062001.
106 D. N. Dirin and M. V. Kovalenko, *Chimia*, 2024, **78**, 862–868.
107 J. Shamsi, A. S. Urban, M. Imran, L. De Trizio and L. Manna, *Chem. Rev.*, 2019, **119**, 3296–3348.
108 D. Choi, H. Kim, Y. Bae, S. Lim and T. Park, *ACS Energy Lett.*, 2024, **9**, 2633–2658.
109 H. Utzat, W. Sun, A. E. K. Kaplan, F. Krieg, M. Ginterseder, B. Spokoyny, N. D. Klein, K. E. Shulenberger, C. F. Perkinson, M. V. Kovalenko and M. G. Bawendi, *Science*, 2019, **363**, 1068–1072.
110 Z. Liu, H. Yang, J. Wang, Y. Yuan, K. Hills-Kimball, T. Cai, P. Wang, A. Tang and O. Chen, *Nano Lett.*, 2021, **21**, 1620–1627.
111 Z. Huang, X. Li, M. Mahboub, K. M. Hanson, V. M. Nichols, H. Le, M. L. Tang and C. J. Bardeen, *Nano Lett.*, 2015, **15**, 5552–5557.
112 M. Wu, D. N. Congreve, M. W. B. Wilson, J. Jean, N. Geva, M. Welborn, T. Van Voorhis, V. Bulović, M. G. Bawendi and M. A. Baldo, *Nat. Photonics*, 2016, **10**, 31–34.
113 X. Li, Z. Huang, R. Zavala and M. L. Tang, *J. Phys. Chem. Lett.*, 2016, **7**, 1955–1959.
114 Z. Xu, Z. Huang, T. Jin, T. Lian and M. L. Tang, *Acc. Chem. Res.*, 2021, **54**, 70–80.
115 Z. Huang, X. Li, B. D. Yip, J. M. Rubalcava, C. J. Bardeen and M. L. Tang, *Chem. Mater.*, 2015, **27**, 7503–7507.
116 X. Li, A. Fast, Z. Huang, D. A. Fishman and M. L. Tang, *Angew. Chem., Int. Ed.*, 2017, **56**, 5598–5602.
117 Z. A. Vanorman, A. S. Bieber, S. Wieghold and L. Nienhaus, *Chem. Mater.*, 2020, **32**, 4734–4742.

118 A. Ronchi, C. Capitani, V. Pinchetti, G. Gariano, M. L. Zaffalon, F. Meinardi, S. Brovelli and A. Monguzzi, *Adv. Mater.*, 2020, **32**, 2002953.
119 E. M. Rigsby, T. Miyashita, D. A. Fishman, S. T. Roberts and M. L. Tang, *RSC Adv.*, 2021, **11**, 31042–31046.
120 M. Mahboub, Z. Huang and M. L. Tang, *Nano Lett.*, 2016, **16**, 7169–7175.
121 Z. Huang, Z. Xu, M. Mahboub, Z. Liang, P. Jaimes, P. Xia, K. R. Graham, M. L. Tang and T. Lian, *J. Am. Chem. Soc.*, 2019, **141**, 9769–9772.
122 J. Schwan, K. Wang, M. L. Tang and L. Mangolini, *Nanoscale*, 2022, **14**, 17385–17391.
123 K. Okumura, N. Yanai and N. Kimizuka, *Chem. Lett.*, 2019, **48**, 1347–1350.
124 S. Ji, W. Wu, W. Wu, H. Guo and J. Zhao, *Angew. Chem., Int. Ed.*, 2011, **50**, 1626–1629.
125 A. Monguzzi, R. Tubino, S. Hoseinkhani, M. Campione and F. Meinardi, *Phys. Chem. Chem. Phys.*, 2012, **14**, 4322–4332.
126 T. Ogawa, N. Yanai, H. Kouno and N. Kimizuka, *J. Photonics Energy*, 2017, **8**, 022003.
127 L. Wei, C. Fan, M. Rao, F. Gao, C. He, Y. Sun, S. Zhu, Q. He, C. Yang and W. Wu, *Mater. Horiz.*, 2022, **9**, 3048–3056.
128 B. Wang, B. Sun, X. Wang, C. Ye, P. Ding, Z. Liang, Z. Chen, X. Tao and L. Wu, *J. Phys. Chem. C*, 2014, **118**, 1417–1425.
129 F. Deng, J. R. Sommer, M. Myahkostupov, K. S. Schanze and F. N. Castellano, *Chem. Commun.*, 2013, **49**, 7406–7408.
130 C. Mongin, J. H. Golden and F. N. Castellano, *ACS Appl. Mater. Interfaces*, 2016, **8**, 24038–24048.
131 N. A. Durandin, J. Isokuortti, A. Efimov, E. Vuorimaa-Laukkanen, N. V. Tkachenko and T. Laaksonen, *Chem. Commun.*, 2018, **54**, 14029–14032.
132 Y. Lu, N. McGoldrick, F. Murphy, B. Twamley, X. Cui, C. Delaney, G. M. Ó. Máille, J. Wang, J. Zhao and S. M. Draper, *Chem.–Eur. J.*, 2016, **22**, 11349–11356.
133 N. Harada, Y. Sasaki, M. Hosoyamada, N. Kimizuka and N. Yanai, *Angew. Chem.*, 2021, **133**, 144–149.
134 F. Glaser, C. Kerzig and O. S. Wenger, *Chem. Sci.*, 2021, **12**, 9922–9933.
135 L. Huang, Y. Zhao, H. Zhang, K. Huang, J. Yang and G. Han, *Angew. Chem.*, 2017, **129**, 14592–14596.
136 A. Olesund, J. Johnsson, F. Edhborg, S. Ghasemi, K. Moth-Poulsen and B. Albinsson, *J. Am. Chem. Soc.*, 2022, **144**, 3706–3716.
137 T. Miyashita, P. Jaimes, T. Lian, M. L. Tang and Z. Xu, *J. Phys. Chem. Lett.*, 2022, **13**, 3002–3007.
138 Z. Q. You and C. P. Hsu, *Int. J. Quantum Chem.*, 2014, **114**, 102–115.
139 Z. Huang and M. L. Tang, *J. Am. Chem. Soc.*, 2017, **139**, 9412–9418.
140 T. Miyashita, S. He, P. Jaimes, A. L. Kaledin, M. Fumanal, T. Lian and M. Lee Tang, *J. Chem. Phys.*, 2024, **161**, 094707.
141 N. Tripathi, M. Ando, T. Akai and K. Kamada, *ACS Appl. Nano Mater.*, 2021, **4**, 9680–9688.
142 Z. Xu, T. Jin, Y. Huang, K. Mulla, F. A. Evangelista, E. Egap and T. Lian, *Chem. Sci.*, 2019, **10**, 6120–6124.
143 M. Koharagi, N. Harada, K. Okumura, J. Miyano, S. Hisamitsu, N. Kimizuka and N. Yanai, *Nanoscale*, 2021, **13**, 19890–19893.
144 J. A. Bender, E. K. Raulerson, X. Li, T. Goldzak, P. Xia, T. Van Voorhis, M. L. Tang and S. T. Roberts, *J. Am. Chem. Soc.*, 2018, **140**, 7543–7553.
145 C. J. Imperiale, F. Yarur Villanueva, E. Nikbin, J. Y. Howe and M. W. B. Wilson, *Chem. Mater.*, 2024, **36**, 4121–4134.
146 M. Mahboub, H. Maghsoudiganjeh, A. M. Pham, Z. Huang and M. L. Tang, *Adv. Funct. Mater.*, 2016, **26**, 6091–6097.
147 X. Luo, R. Lai, Y. Li, G. Liang, X. Liu, T. Ding, J. Wang and K. Wu, *J. Am. Chem. Soc.*, 2019, **141**(10), 4186–4190.
148 R. Weiss, Z. A. VanOrman, C. M. Sullivan and L. Nienhaus, *ACS Mater. Au*, 2022, **2**, 641–654.
149 M. Mahboub, P. Xia, J. Van Baren, X. Li, C. H. Lui and M. L. Tang, *ACS Energy Lett.*, 2018, **3**, 767–772.
150 S. Brkić, *Optical Properties of Quantum Dots*, 2016.
151 K. Mase, K. Okumura, N. Yanai and N. Kimizuka, *Chem. Commun.*, 2017, **53**, 8261–8264.
152 F. Y. Villanueva, M. Hasham, P. B. Green, C. J. Imperiale, S. Rahman, D. C. Burns and M. W. B. Wilson, *ACS Nano*, 2024, **18**, 35182–35201.
153 I. Moreels, Y. Justo, B. De Geyter, K. Haustraete, J. C. Martins and Z. Hens, *ACS Nano*, 2011, **5**, 2004–2012.
154 Q. A. Akkerman and L. Manna, *ACS Energy Lett.*, 2020, **5**, 604–610.
155 M. A. Becker, R. Vaxenburg, G. Nedelcu, P. C. Sercel, A. Shabaev, M. J. Mehl, J. G. Michopoulos, S. G. Lambrakos, N. Bernstein, J. L. Lyons, T. Stöferle, R. F. Mahrt, M. V. Kovalenko, D. J. Norris, G. Rainò and A. L. Efros, *Nature*, 2018, **553**, 189–193.
156 J. Chakkamalayath and P. V. Kamat, *J. Am. Chem. Soc.*, 2024, **146**, 18095–18103.
157 A. Chemmangat, J. Chakkamalayath, J. T. DuBose and P. V. Kamat, *J. Am. Chem. Soc.*, 2024, **146**, 3352–3362.
158 H. Cheng, S. Ding, M. Hao, L. Wang and J. A. Steele, *Next Energy*, 2024, **4**, 100152.
159 J. Kolny-Olesiak and H. Weller, *ACS Appl. Mater. Interfaces*, 2013, **5**, 12221–12237.
160 M. Huang, X. Cai, Q. Shan, L. Yang, T. Hu, Y. Wang, X. Chen and H. Zeng, *J. Lumin.*, 2025, **281**, 121136.
161 H. Zang, H. Li, N. S. Makarov, K. A. Velizhanin, K. Wu, Y. S. Park and V. I. Klimov, *Nano Lett.*, 2017, **17**, 1787–1795.
162 Y.-H. Ko, P. Prabhakaran, S. Choi, G.-J. Kim, C. Lee and K.-S. Lee, *Sci. Rep.*, 2020, **10**, 15817.
163 T. S. Ponomaryova, A. S. Novikova, A. M. Abramova, O. A. Goryacheva, D. D. Drozd, P. D. Strokin and I. Y. Goryacheva, *J. Anal. Chem.*, 2022, **77**, 402–409.
164 A. C. Berends, M. J. J. Mangnus, C. Xia, F. T. Rabouw and C. De Mello Donega, *J. Phys. Chem. Lett.*, 2019, **10**, 1600–1616.
165 Y. Xia, N. Kapuria, M. He, U. V. Ghorpade, X. Guo, B. Hao, S. W. Shin, Z. Hameiri, X. Hao and M. P. Suryawanshi, *Adv. Powder Mater.*, 2025, 100283.
166 S. Morozova, M. Alikina, A. Vinogradov and M. Pagliaro, *Front. Chem.*, 2020, **8**, 191.
167 B. Chen, D. Li and F. Wang, *Small*, 2020, **16**, 2002454.

168 O. Voznyy, L. Levina, J. Z. Fan, M. Askerka, A. Jain, M. J. Choi, O. Ouellette, P. Todorović, L. K. Sagar and E. H. Sargent, *ACS Nano*, 2019, **13**, 11122–11128.
169 M. K. Manna, S. Shokri, G. P. Wiederrecht, D. J. Gosztola and A. J. L. Ayitou, *Chem. Commun.*, 2018, **54**, 5809–5818.
170 C. M. Sullivan and L. Nienhaus, *Chimia*, 2024, **78**, 518–524.
171 A. Shamirian, H. Samareh Afsari, A. Hassan, L. W. Miller and P. T. Snee, *ACS Sens.*, 2016, **1**, 1244–1250.
172 P. Ziółczyk, K. Kur-Kowalska, M. Przybyt and E. Miller, *Spectrochim. Acta, Part A*, 2014, **126**, 28–35.
173 N. Tripathi and K. Kamada, *ACS Appl. Nano Mater.*, 2024, **7**, 2950–2955.
174 D. K. Limberg, J. H. Kang and R. C. Hayward, *J. Am. Chem. Soc.*, 2022, **144**, 5226–5232.
175 Q. Dou, L. Jiang, D. Kai, C. Owh and X. J. Loh, *Drug Discovery Today*, 2017, **22**, 1400–1411.
176 B. S. Richards, D. Hudry, D. Busko, A. Turshatov and I. A. Howard, *Chem. Rev.*, 2021, **121**, 9165–9195.
177 D. Beery, J. P. Wheeler, A. Arcidiacono and K. Hanson, *ACS Appl. Energy Mater.*, 2020, **3**, 29–37.
178 F. Glaser, C. Kerzig and O. S. Wenger, *Angew. Chem., Int. Ed.*, 2020, **59**, 10266–10284.
179 B. D. Ravetz, A. B. Pun, E. M. Churchill, D. N. Congreve, T. Rovis and L. M. Campos, *Nature*, 2019, **565**, 343–346.
180 M. Barawi, F. Fresno, R. Pérez-Ruiz and V. A. De La Peña O'Shea, *ACS Appl. Energy Mater.*, 2019, **2**, 207–211.
181 N. Awwad, A. T. Bui, E. O. Danilov and F. N. Castellano, *Chem*, 2020, **6**, 3071–3085.
182 M. Majek, U. Faltermeier, B. Dick, R. Pérez-Ruiz and A. Jacobi von Wangelin, *Chem.–Eur. J.*, 2015, **21**, 15496–15501.
183 B. Pfund, D. M. Steffen, M. R. Schreier, M. S. Bertrams, C. Ye, K. Börjesson, O. S. Wenger and C. Kerzig, *J. Am. Chem. Soc.*, 2020, **142**, 10468–10476.
184 S. Liu, H. Liu, Y. Hu, C. Zhao, H. Huang, G. Yu, Z. Li, Z. Liu, Y. Chen and X. Li, *Chem. Eng. J.*, 2023, **452**, 139203.
185 B. Shan, T. T. Li, M. K. Brennaman, A. Nayak, L. Wu and T. J. Meyer, *J. Am. Chem. Soc.*, 2019, **141**, 463–471.
186 A. Monguzzi, A. Oertel, D. Braga, A. Riedinger, D. K. Kim, P. N. Knüsel, A. Bianchi, M. Mauri, R. Simonutti, D. J. Norris and F. Meinardi, *ACS Appl. Mater. Interfaces*, 2017, **9**, 40180–40186.
187 E. Madbak, D. J. Osborn, T. Small, T. Ishwara, T. W. Schmidt, K. Domen and G. F. Metha, *Chem. Commun.*, 2025, **61**, 157–160.
188 S. Chandrasekaran, Y. L. T. Ngo, L. Sui, E. J. Kim, D. K. Dang, J. S. Chung and S. H. Hur, *Dalton Trans.*, 2017, **46**, 13912–13919.
189 T. Yu, Y. Liu, Y. Zeng, J. Chen, G. Yang and Y. Li, *Chem.–Eur. J.*, 2019, **25**, 16270–16276.
190 J. Fang, Y. Chen, W. Wang, L. Fang, C. Lu, C. Zhu, J. Kou, Y. Ni and Z. Xu, *Appl. Catal., B*, 2019, **258**, 117762.
191 J. Fang, W. Wang, C. Zhu, L. Fang, J. Jin, Y. Ni, C. Lu and Z. Xu, *Appl. Catal., B*, 2017, **217**, 100–107.
192 D. Choi, S. Kyung Nam, K. iwon Kim, J. Moon, D. Choi, S. K. Nam, K. Kim and J. H. Moon, *Angew. Chem., Int. Ed.*, 2019, **58**, 6891–6895.
193 P. Venkatesan, J. Y. Lin, D. Roy, P. Aloni, Z. F. Lin and R. A. Doong, *Appl. Catal. B Environ. Energy*, 2025, **365**, 124913.
194 J. H. Kim and J. H. Kim, *J. Am. Chem. Soc.*, 2012, **134**, 17478–17481.
195 O. S. Kwon, J.-H. Kim, J. K. Cho and J.-H. Kim, *ACS Appl. Mater. Interfaces*, 2015, **7**, 318–325.
196 H. Il Kim, O. S. Kwon, S. Kim, W. Choi and J. H. Kim, *Energy Environ. Sci.*, 2016, **9**, 1063–1073.
197 A. L. Hagstrom, S. Weon, W. Choi and J. H. Kim, *ACS Appl. Mater. Interfaces*, 2019, **11**, 13304–13318.
198 S. Liu, H. Liu, L. Shen, Z. Xiao, Y. Hu, J. Zhou, X. Wang, Z. Liu, Z. Li and X. Li, *Chem. Eng. J.*, 2022, **431**, 133377.
199 L. Huang, W. Wu, Y. Li, K. Huang, L. Zeng, W. Lin and G. Han, *J. Am. Chem. Soc.*, 2020, **142**, 18460–18470.
200 A. Monguzzi, D. Braga, M. Gandini, V. C. Holmberg, D. K. Kim, A. Sahu, D. J. Norris and F. Meinardi, *Nano Lett.*, 2014, **14**, 6644–6650.
201 S. Rühle, *Sol. Energy*, 2016, **130**, 139–147.
202 A. J. Carrod, V. Gray and K. Börjesson, *Energy Environ. Sci.*, 2022, **15**, 4982–5016.
203 Y. Y. Cheng, A. Nattestad, T. F. Schulze, R. W. Macqueen, B. Fückel, K. Lips, G. G. Wallace, T. Khoury, M. J. Crossley and T. W. Schmidt, *Chem. Sci.*, 2016, **7**, 559–568.
204 A. Nattestad, Y. Y. Cheng, R. W. Macqueen, T. F. Schulze, F. W. Thompson, A. J. Mozer, B. Fückel, T. Khoury, M. J. Crossley, K. Lips, G. G. Wallace and T. W. Schmidt, *J. Phys. Chem. Lett.*, 2013, **4**, 2073–2078.
205 S. N. Sanders, T. H. Schloemer, M. K. Gangishetty, D. Anderson, M. Seitz, A. O. Gallegos, R. C. Stokes and D. N. Congreve, *Nature*, 2022, **604**, 474–478.
206 M. Wu, T.-A. Lin, J. O. Tiepelt, V. Bulović and M. A. Baldo, *Nano Lett.*, 2021, **21**, 1011–1016.
207 S. P. Hill and K. Hanson, *J. Am. Chem. Soc.*, 2017, **139**, 10988–10991.
208 M. P. Rauch and R. R. Knowles, *Chimia*, 2018, **72**, 501–507.
209 H. L. Lee, J. H. Park, H. S. Choe, M. S. Lee, J. M. Park, N. Harada, Y. Sasaki, N. Yanai, N. Kimizuka, J. Zhu, S. H. Bhang and J. H. Kim, *ACS Appl. Mater. Interfaces*, 2019, **11**, 26571–26580.
210 R. Zhang, Y. Guan, Z. Zhu, H. Lv, F. Li, S. Sun and J. Li, *ACS Appl. Mater. Interfaces*, 2019, **11**, 37479–37490.
211 Y. Peng, J.-Y. Li, F. Qi, D.-X. Guo, Y.-Z. Li, H.-J. Feng, L.-H. Jiang, M.-Y. Zhang, Y.-X. Liu, L. Zeng and L. Huang, *Nano Lett.*, 2025, **25**, 5291–5298.
212 C. J. O'Dea, J. Isokuortti, E. E. Comer, S. T. Roberts and Z. A. Page, *ACS Cent. Sci.*, 2024, **10**, 272–282.
213 J. Wong, S. Wei, R. Meir, N. Sadaba, N. A. Ballinger, E. K. Harmon, X. Gao, G. Altin-Yavuzarslan, L. D. Pozzo, L. M. Campos and A. Nelson, *Adv. Mater.*, 2023, **35**, 2207673.
214 R. Forecast, F. Campaioli, T. W. Schmidt and J. H. Cole, *J. Phys. Chem. A*, 2023, **127**, 1794–1800.
215 L. Huang, T. Le, K. Huang and G. Han, *Nat. Commun.*, 2021, **121**, 1–9.

216 S. Amemori, R. K. Gupta, M. L. Böhm, J. Xiao, U. Huynh, T. Oyama, K. Kaneko, A. Rao, N. Yanai and N. Kimizuka, *Dalton Trans.*, 2018, **47**, 8590–8594.
217 A. Brion, J. Chaud, M. Klimezak, F. Bolze, L. Ohlmann, J. Léonard, S. Chassaing, B. Frisch, A. Kichler, B. Heurtault and A. Specht, *Bioconjug. Chem.*, 2023, **34**, 1304–1315.
218 H. Yang, S. Guo, B. Jin, Y. Luo and X. Li, *Polym. Chem.*, 2022, **13**, 4887–4894.
219 F. Saenz, A. Ronchi, M. Mauri, D. Kiebala, A. Monguzzi and C. Weder, *ACS Appl. Mater. Interfaces*, 2021, **13**, 43314–43322.
220 H. Lee, M. S. Lee, M. Uji, N. Harada, J. M. Park, J. Lee, S. E. Seo, C. S. Park, J. Kim, S. J. Park, S. H. Bhang, N. Yanai, N. Kimizuka, O. S. Kwon and J. H. Kim, *ACS Appl. Mater. Interfaces*, 2022, **14**, 4132–4143.
221 Q. Wang and D. Astruc, *Chem. Rev.*, 2020, **120**, 1438–1511.
222 S. Gharaati, C. Wang, C. Förster, F. Weigert, U. Resch-Genger and K. Heinze, *Chem.–Eur. J.*, 2020, **26**, 1003–1007.
223 F. Qi, H.-J. Feng, J.-Y. Li, Y. Peng, L.-H. Jiang, Y.-Z. Li, L. Zeng and L. Huang, *Small Methods*, 2025, 2401945.
224 S. E. Seo, H. S. Choe, H. Cho, H. Il Kim, J. H. Kim and O. S. Kwon, *J. Mater. Chem. C*, 2022, **10**, 4483–4496.
225 D. Di, L. Yang, J. M. Richter, L. Meraldi, R. M. Altamimi, A. Y. Alyamani, D. Credgington, K. P. Musselman, J. L. MacManus-Driscoll, R. H. Friend, D. Di, L. Yang, J. M. Richter, L. Meraldi, D. Credgington, R. H. Friend, R. M. Altamimi, A. Y. Alyamani, K. P. Musselman and J. L. MacManus-Driscoll, *Adv. Mater.*, 2017, **29**, 1605987.
226 T. Miteva, V. Yakutkin, G. Nelles and S. Baluschev, *New J. Phys.*, 2008, **10**, 103002.
227 N. Geva, L. Nienhaus, M. Wu, V. Bulović, M. A. Baldo, T. Van Voorhis and M. G. Bawendi, *J. Phys. Chem. Lett.*, 2019, **10**, 3147–3152.
228 P. Baronas, J. Lekavičius, M. Majdecki, J. L. Elholm, K. Kazlauskas, P. Gaweł and K. Moth-Poulsen, *ACS Cent. Sci.*, 2025, **11**, 413–421.